

Review

# Review: Heterojunction Tandem Solar Cells on Si-Based Metal Oxides

Laurentiu Fara <sup>1,2,\*</sup> , Irinela Chilibon <sup>3</sup>, Dan Craciunescu <sup>1</sup>, Alexandru Diaconu <sup>1</sup> and Silvian Fara <sup>1</sup>

<sup>1</sup> Department of Physics, Faculty of Applied Sciences, Polytechnic University of Bucharest, 060042 Bucharest, Romania; dan.craciunescu@sdeftib.pub.ro (D.C.)

<sup>2</sup> Academy of Romanian Scientists, 050091 Bucharest, Romania

<sup>3</sup> Development for Optoelectronics (INOE-2000), National Institute of Research, 077125 Magurele, Romania

\* Correspondence: lfara@renerg.pub.ro

**Abstract:** PV technology offers a sustainable solution to the increased energy demand especially based on mono- and polycrystalline silicon solar cells. The most recent years have allowed the successful development of perovskite and tandem heterojunction Si-based solar cells with energy conversion efficiency over 28%. The metal oxide heterojunction tandem solar cells have a great potential application in the future photovoltaic field. Cu<sub>2</sub>O (band gap of 2.07 eV) and ZnO (band gap of 3.3 eV) are very good materials for solar cells and their features completely justify the high interest for the research of tandem heterojunction based on them. This review article analyzes high-efficiency silicon-based tandem heterojunction solar cells (HTSCs) with metal oxides. It is structured on six chapters dedicated to four main issues: (1) fabrication techniques and device architecture; (2) characterization of Cu<sub>2</sub>O and ZnO layers; (3) numerical modelling of Cu<sub>2</sub>O/ZnO HTSC; (4) stability and reliability approach. The device architecture establishes that the HTSC is constituted from two sub-cells: ZnO/Cu<sub>2</sub>O and c-Si. The four terminal tandem solar cells contribute to the increased current density and conversion efficiency. Cu<sub>2</sub>O and ZnO materials are defined as promising candidates for high-efficiency solar devices due to the morphological, structural, and optical characterization emphasized. Based on multiscale modelling of PV technology, the electrical and optical numerical modelling of the two sub-cells of HTSC are presented. At the same time, the thermal stability and reliability approach are essential and needed for an optimum operation of HTSC, concerning the cell lifetime and degradation degree. Further progress on flexible HTSC could determine that such advanced solar devices would become commercially sustainable in the near future.

**Keywords:** tandem heterojunction solar cell (HTSC); metal oxides; four terminals; morphological; structural and optical characterization; modelling and simulation; stability and reliability



**Citation:** Fara, L.; Chilibon, I.; Craciunescu, D.; Diaconu, A.; Fara, S. Review: Heterojunction Tandem Solar Cells on Si-Based Metal Oxides. *Energies* **2023**, *16*, 3033. <https://doi.org/10.3390/en16073033>

Academic Editor: Philippe Leclère

Received: 20 December 2022

Revised: 7 February 2023

Accepted: 10 March 2023

Published: 26 March 2023



**Copyright:** © 2023 by the authors. Licensee MDPI, Basel, Switzerland. This article is an open access article distributed under the terms and conditions of the Creative Commons Attribution (CC BY) license (<https://creativecommons.org/licenses/by/4.0/>).

## 1. Introduction

In the present era, the leading role in the increase of renewable energy production on a global scale is played by the public company sector of the European Union (EU) and is represented by 20% of energy needs based on renewables reached by national targets [1,2]. In the near future, the EU could become a global leader in renewable energy (see the revised “Directive of the European Parliament and of the Council on the promotion of the use of energy from Renewable Sources” [3]) and would ensure at least 27% renewables (RE) in the final EU energy consumption and possibly 35% RE in the total energy consumption by 2030. Taking into account that the photovoltaics (PV) could have a leading role in the RE global scale, their cost would drop significantly [4]. The number of PV installations would be increased and that would drive the cost of PV down. Based on essential reports of (1) the International Energy Agency Photovoltaic Power System Programme (IEA PVPS) [5]; (2) the Renewable Energy Policy for the 21st Century (REN21) [6]; and (3) Joint Research Centre (JRC) of the European Commission (EC) [7], the PV market is growing more and

more, especially in China and India. A very good example is highlighted by the organic photovoltaic (OPV) technology that could compete with the conventional technologies in both roof- and ground-mounted systems [8]. The gap between theoretical limits of solar cell efficiencies and those determined at the laboratory scale, as well as at the industrial level, has obtained an increased incentive that would allow the experimental efficiencies to reach the calculated theoretical limits. At the same time, new materials for advanced solar cells with an emphasis on cost, performance, and environmental aspects were developed [9,10]. Metal oxide heterojunction tandem solar devices could be considered more advantageous in comparison with DSSC and OPV solar cells due to their very good qualities (accessible, non-expensive, non-polluting, and easy exploiting) [11]. Cuprous oxide ( $\text{Cu}_2\text{O}$ ) is a very attractive candidate based on its special features: direct forbidden bandgap, strong absorption of visible light, and high minority carrier diffusion length [12,13]; it could act as an efficient solar absorber layer. An important drawback of such a layer is determined by its intrinsic defects (copper vacancies and oxygen interstitials), as well as low solubility of doping impurities [14]. c-Si-based tandem solar cells are of special interest for the PV community. However, some types of top solar cells have clear qualities but also present certain drawbacks. III-V/Si tandem solar cells exhibit important high efficiency and stability, but have a high manufacturing cost. Perovskites/Si tandem developed rapidly and achieved 30% efficiency, but present low stability in an outdoor environment. That is why  $\text{Cu}_2\text{O}/\text{Si}$  tandem has an acceptable high theoretical efficiency, decent stability, earth-abundant raw material to reduce costs, and development prospects based on good device performance.

Special research was explored to find corresponding n-type oxides for heterojunction  $\text{Cu}_2\text{O}$ -based solar cells [15–17]. A very interesting tandem heterojunction solar cell configuration is represented by a  $\text{ZnO}(\text{AZO})/\text{Cu}_2\text{O}$  top sub-cell combined with a c-Si bottom sub-cell [18,19]. The main merits of a such a combination would be (1) large scale availability; (2) non-toxicity; (3) plenty of material. The remarkable qualities of a ZnO layer could be defined by (1) direct band gap of 3.3 eV; (2) large exciton binding energy of 60 meV at room temperature; (3) high electron diffusivity; (4) high electrical conductivity.

*The exciton binding energy of 60 meV at room temperature* is a unique property of ZnO. This means ZnO can emit light effectively. It is remarked that for emitted material, the larger exciton binding energy, the stronger the interaction between the electron and hole. It means the rate of emitted recombination is easier and therefore this is an important property when it is considered optical material.

Thin film solar cells based on  $\text{Cu}_2\text{O}/\text{ZnO}$  heterojunction were selected as an excellent candidate for future generations of solar cells with a maximum reported conversion efficiency of 8.1% [20,21] and an estimated theoretical efficiency of 30% depending upon the optical absorption,  $E_g$ , carrier transfer, and luminescence efficiency of the top sub-cell [22,23].

Copper oxide semiconducting material including its band structure and the method of the production of  $\text{Cu}_2\text{O}$  has a high applicability for solar cells [12,13,16,18–20,24]. A deep analysis reveals that (1) the high resistivity of starting material is responsible for the low value of electrical power conversion efficiency of  $\text{Cu}_2\text{O}$ -based solar cells. (2) Non-existence of a technique of doping  $\text{Cu}_2\text{O}$  to obtain a low resistivity n-type semiconductor allows conversion efficiencies greater than 2% for p-n homo-junction  $\text{Cu}_2\text{O}$  solar cell to be fabricated. (3) A copper copper-rich or oxygen-deficient surface makes all Schottky barriers essentially a  $\text{Cu}/\text{Cu}_2\text{O}$  structure. The copper oxide-based semiconductors fulfill the most important criteria of the future progress: availability, sustainability, non-toxicity (elements of hope), and ease of synthesis.

*The organization* of this paper is based on the correlation of the following essential HTSC items, namely: (1) solar device architecture; (2) fabrication techniques of  $\text{Cu}_2\text{O}$ , ZnO and  $\text{Cu}_2\text{O}/\text{ZnO}$  heterojunction; (3) characterization of  $\text{Cu}_2\text{O}$  and ZnO layer structures; (4) modelling and simulation (electrical and optical) of HTSC with  $\text{Cu}_2\text{O}/\text{ZnO}$  heterojunction; (5) stability and reliability approach.

The main objective of this article is determined by a unified approach of HTSC with the stress on three main features: (1) fabrication and characterization of  $\text{Cu}_2\text{O}$  and  $\text{ZnO}$  structures; (2) numerical modelling; and (3) stability and reliability.

Another objective is to highlight the N-doped cuprous oxide heterojunction solar cell as a promising candidate for high-efficiency solar devices.

## 2. Fabrication Techniques and Device Architecture

### 2.1. Basics on Tandem Devices

The maximum absorbed solar energy can be obtained by stacking several tandem junctions with different bandgaps.

The maximum theoretical conversion efficiency of corresponding solar tandem devices is: (a) 44% (two junctions), 54% (three junctions), and 66% (infinite number of junctions) for non-concentrated solar radiation [25];

(b) 55% (two junctions), 63% (three junctions), and 86% (infinite number of junctions) for concentrated solar radiation [26].

Multi-junction experimental tandem solar cells presented a high conversion efficiency of: (a) 46% with four junctions and concentrated solar radiation, and (b) 38.8% with four junctions and non-concentrated solar radiation [27].

The best possible  $\text{ZnO}/\text{Cu}_2\text{O}$  tandem heterojunction would be obtained with an optimized  $\text{Cu}_2\text{O}$  layer deposited on glass substrate under different conditions [24].

### 2.2. Device Architecture

One of the main directions for the development of high-efficiency solar cells is research on HTSCs based on silicon and metal oxides. Figure 1 presents the device structure of two Quartz/AZO( $\text{ZnO}$ )/ $\text{Cu}_2\text{O}$  sub-cell patterns with copper contacts.

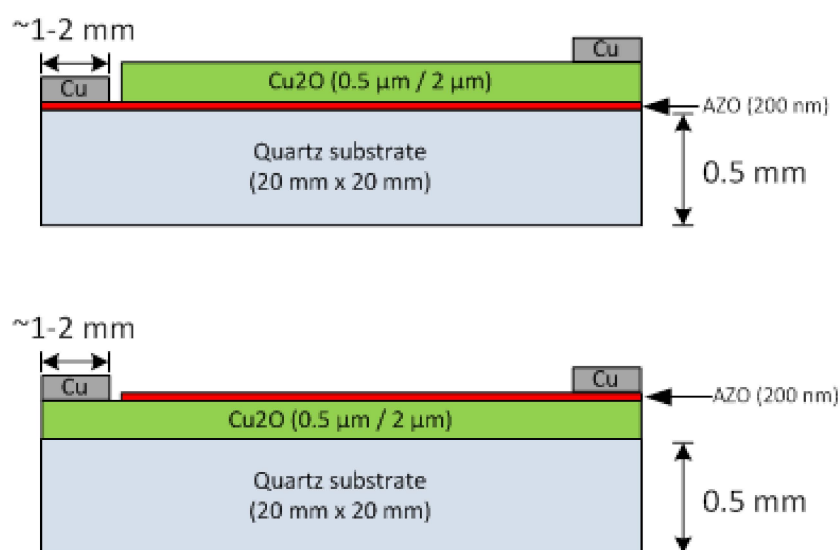
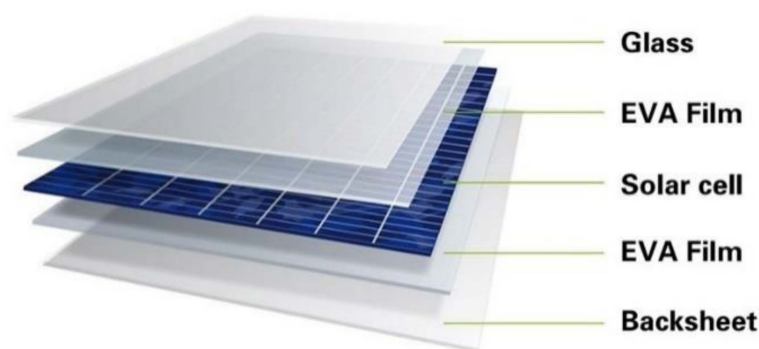
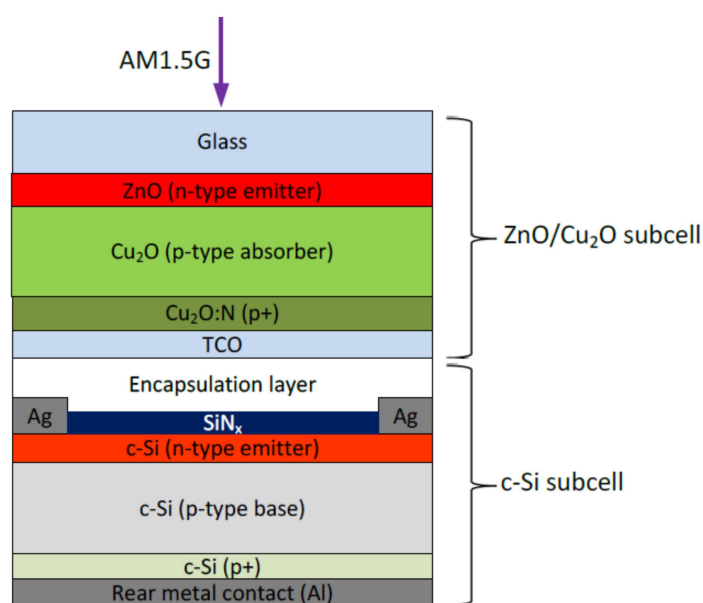


Figure 1. Solar top sub-cell patterns in the tandem structure [18].

Reactive MSP of metal oxides on a transparent glass (quartz) substrate realizes the  $\text{ZnO}/\text{Cu}_2\text{O}$  sub-cell allowing low energy photons to be transmitted through the top AZO ( $\text{ZnO}$ )/ $\text{Cu}_2\text{O}$  sub-cell for corresponding absorption in the bottom c-Si sub-cell. The  $\text{ZnO}/\text{Cu}_2\text{O}$  top sub-cell deposited on the glass encapsulates the c-Si bottom sub-cell (see Figure 2). In Figure 3, a schematic device design of a four-terminal tandem solar cell combines into a stack a conventional Si sub-cell with a  $\text{ZnO}/\text{Cu}_2\text{O}$  sub-cell. The four-terminal tandem solar cell compared to the conventional two-terminal solar cell contributes to the increase of current density and conversion efficiency.



**Figure 2.** Method for laminating the Quartz/AZO/Cu<sub>2</sub>O to a c-Si bottom cell in order to form a device with four-terminal contacts [19].



**Figure 3.** Schematic device design of a four-terminal tandem heterojunction solar cell combining a conventional crystalline Si as bottom sub-cell with a metal oxide top sub-cell based on ZnO and Cu<sub>2</sub>O layers [20].

A device called the IBSC (Intermediate Band Solar Cell) was proposed for the increasing of maximum theoretical efficiency of solar cells. Nitrogen is a good dopant that could be used to make an IB material from Cu<sub>2</sub>O. It should be simple to dope the Cu<sub>2</sub>O with nitrogen in a large concentration, and it has been shown to be a good p-type dopant.

Nitrogen-doped cuprous oxide is the selected candidate material with an intermediate band, in conjunction with ZnO, respectively, ZnO/N: Cu<sub>2</sub>O. The obtained major challenges would be (1) the production of monocrystalline Cu<sub>2</sub>O; (2) low resistivity of Cu<sub>2</sub>O; and (3) charge transport and recombination at the AZO/Cu<sub>2</sub>O interface. Cu<sub>2</sub>O and AZO have to be deposited with high crystalline quality and low resistivity [24]. Cu<sub>2</sub>O and AZO thin films are deposited on quartz substrates by (DC/RF) MSS. Cu<sub>2</sub>O is deposited by reactive sputtering of a Cu target in O<sub>2</sub>/Ar with 400 °C substrate temperature, and fixed power density. To improve the optical and electrical properties, the grown Cu<sub>2</sub>O films are annealed at 900 °C in vacuum. AZO is deposited by co-sputtering of pure ZnO ceramic target and Al target in Ar with 400 °C substrate temperature [28].

### 2.3. Cu<sub>2</sub>O Fabrication Techniques

The reported Cu<sub>2</sub>O-based structures have employed Cu<sub>2</sub>O sheets realized by Cu thermal oxidation [29].

Cu<sub>2</sub>O films could be deposited by different methods, respectively: Magnetron Sputtering (MSP) [30], Electro-Chemical Deposition (ECD) [31], Plasma-enhanced Atomic Layer Deposition/Pulsed Laser Deposition (ALD/PLD) [32,33], Photochemical Deposition [34], Metal Organic Chemical Vapor Deposition (MOCVD) [35], sol-gel technique [36], and others. Presented shortly are a few **Deposition Methods**, including their *Advantages and Disadvantages*.

#### A. Pulsed Laser Deposition (PLD) [37]

Pulsed Laser Deposition (PLD), also known as Pulsed Laser Ablation (PLA), uses a laser to bombard the surface of the target, raising its surface temperature and further producing high temperature and high pressure plasma ( $T > 104$  K), depositing on different substrates to form a film. *Advantages*: (a) It is easy to obtain by PLD multi-component film of desired stoichiometric ratio. (b) It has high deposition rate, short test period, and low substrate temperature. (c) The process is simple and flexible with great development potential and great compatibility. (d) The process parameters can be arbitrarily adjusted. Multi-target components are flexible. (e) It is easy to clean and prepare a variety of thin film materials. (f) PLD uses UV pulsed laser of high photon capability and high energy density as energy source for plasma generation, so it is non-polluting and easy to control. (g) PLD is suitable for applications in microelectronics, sensor technology, and new material films. *Disadvantages*: (a) For several materials, there are molten small particles or target fragments in the deposited film, which are sputtered during the laser-induced explosion and reduce the quality of the film. (b) The feasibility of the laser method for large area deposition has not been proved yet. (c) Average deposition rate of PLD is slow.

#### B. Magnetron Sputtering (MSP) [38]

Magnetron sputtering is the main thin film deposition method for manufacturing semiconductors, disk drives, CDs, and optical devices. *Advantages*: (a) The deposition speed of MSP is fast, the requirement of substrate temperature rise is low, and the damage to the film is small. (b) For most materials, they can be coated by MSP. (c) The bonding performance between the thin film and the substrate obtained by MSP is good. (d) The thin film obtained by MSP has high purity, good density, and good film formation uniformity. (e) The repeatability of the MSP is good, and a thin film with a uniform thickness can be obtained on a large area substrate. (f) The thickness of the coating and the particle size of the constituent thin film can be controlled by changing parameter conditions. (g) Different metals, alloys, and oxides can be mixed and sputtered on the substrate at the same time. (h) It is easy to realize industrialization.

*Disadvantages*: (a) The sputtering gas, argon, emits a strong light blue glow forming a halo. The target under the halo is severely bombarded by ions, and a ring-shaped groove is sputtered. (b) The plasma is unstable. (c) Low temperature and high-speed sputtering of ferromagnetic materials cannot be realized. It is not possible to add an external magnetic field near the target.

#### C. Metal Organic Chemical Vapor Deposition (MOCVD) [39]

MOCVD is a coating process that uses metal ions to create thin film oxides. It can be used to create lead-based ferroelectric layers. The deposition source is a complex metal organic ligand; MOCVD allows extremely low-cost production of lead-based ferroelectric layers. *Advantages*: (a) thin film oxide deposition; (b) design of improved precursors; (c) lead-based ferroelectric layers for uncooled thermal images; (d) preparation of complex ferroelectric oxides. *Disadvantages*: (a) MOCVD precursors are very hazardous and toxic. (b) They are formed of highly toxic and hybrid gases due to the formation of phosphine.

#### D. Plasma-enhanced Atomic Layer Deposition (ALD) [40]

*Atomic Layer Deposition (ALD)* [41] is an ultra-thin film deposition technique that has found many applications due to its special abilities, namely: (1) uniform deposition of films with controllable thickness, and (2) improvement of the efficiency of electronic devices. This technology has attracted significant interest, both for new functional materials to

be synthesized by ALD, and for several practical applications, such as advanced nano-patterning in microelectronics, energy storage systems, desalination, catalysis, and medical use. *Advantages:* (a) Experimental approaches that affect the deposition and present simulation, such as molecular dynamics and computational fluid dynamics. It would predict the optimization of ALD processes and would determine the reduction in cost, energy waste, and adverse environmental impact. (b) The copper oxide films are deposited on silicon substrates by reactive r.f. MSP at 400 °C. (c) The film thickness is measured by ellipsometry [29,42]. (d) Potential applications for Cu<sub>2</sub>O films include specific devices, such as p-Cu<sub>2</sub>O/n-ZnO photodetectors [38] and solar cells [20,39]. (e) After rapid thermal annealing at 900 °C, the electrical properties of Cu<sub>2</sub>O film on quartz are improved by Hall effect measurements [40].

#### 2.4. ZnO Fabrication Techniques

ZnO is a naturally abundant material which crystallizes either in zinc blende (fcc) phase or wurtzite packed phase. The measured photovoltaic properties of ZnO/Cu<sub>2</sub>O HTSC fabricated with thin films deposited on substrates depend on the target orientation, perpendicularly/parallel to the target [43].

AZO thin films are deposited via *spin coating technique* onto glass substrates at 3000 rpm. An undoped ZnO precursor solution is prepared by dissolving acetate dehydrate [ZnAc:(Zn(CH<sub>3</sub>COO)<sub>2</sub>2H<sub>2</sub>O)] in 2-propanol and diethanolamine (DEA, C<sub>4</sub>H<sub>11</sub>NO<sub>2</sub>) [44]. Experimental ZnO thin films are deposited by *ALD technique* at 200 °C. ZnO thin films are grown on Si and fused quartz (SiO<sub>2</sub>) substrates [45]. ZnO as n-type semiconductor is one of the most relevant combinations of II-VI (A<sup>II</sup>B<sup>VI</sup>) [46].

The physical properties of ZnO thin films prepared by MSP are significantly affected by growth parameters such as gas pressure, time, target-to-substrate distance, deposition power, type and substrate temperature, and annealing temperature. The films' temperature and the substrate type on the growth influence the crystal structure, as well as morphological and optical properties of ZnO thin films [46]. ZnO presents essential properties such as high transparency, high electrical conductivity, and high reflectance in IR.

#### 2.5. Fabrication of Cu<sub>2</sub>O/ZnO Heterojunction

The challenges associated with Cu<sub>2</sub>O/ZnO Tandem Heterojunctions (see Table 1) can be identified as follows: (a) They are made under ambient conditions. (b) The measures to reduce Cu<sub>2</sub>O instability result in PCE above 2%. (c) A higher quality interface in the optimized devices improves the open-circuit voltage three-fold.

**Table 1.** Cu<sub>2</sub>O-based solar cell efficiency latest developments (until 2014). This table is based on that proposed by Ievskaya et al. [47].

Type of Junction	PCE %	Voc	Deposition Method	Ref.
Cu <sub>2</sub> O-based junctions developed in vacuum				
AZO/Ga <sub>2</sub> O <sub>3</sub> /Cu <sub>2</sub> O	5.38	0.8	PLD on Cu <sub>2</sub> O sheet	[48]
AZO/Zn <sub>0.91</sub> Mg <sub>0.09</sub> O/Cu <sub>2</sub> O	4.3	0.8	PLD on Cu <sub>2</sub> O sheet	[49]
AZO/ZnO/Cu <sub>2</sub> O	4.12	0.72	PLD on Cu <sub>2</sub> O sheet	[50]
AZO/Ga <sub>2</sub> O <sub>3</sub> /Cu <sub>2</sub> O	3.97	1.2	ALD	[51]
AZO/ZnO/Cu <sub>2</sub> O	3.83	0.69	PLD on Cu <sub>2</sub> O sheet	[52]
AZO/a-ZTO/Cu <sub>2</sub> O	2.85	0.62	ALD	[53]
AZO/a-ZTO/Cu <sub>2</sub> O	2.65	0.55	ALD	[54]
AZO/Cu <sub>2</sub> O	2.53	0.55	PLD on Cu <sub>2</sub> O sheet	[55]
ITO/ZnO/Cu <sub>2</sub> O	2.01	0.6	IBS	[56]
ZnO:Ga/Cu <sub>2</sub> O	1.52	0.41	VAPE	[57]
AZO/Cu <sub>2</sub> O	1.39	0.4	dc-MSP	[57]
AZO/Cu <sub>2</sub> O	1.21	0.41	PLD	[58]
AZO/Cu <sub>2</sub> O	0.24	0.34	electrodeposition	[59]

**Table 1.** *Cont.*

Type of Junction	PCE %	Voc	Deposition Method	Ref.
Cu <sub>2</sub> O-based junctions developed without vacuum				
ZnO/Cu <sub>2</sub> O	0.12	0.19	ECD	[60]
ZnO/Cu <sub>2</sub> O	1.43	0.54	ECD	[61]
ZnO/Cu <sub>2</sub> O	1.28	0.59	ECD	[62]
ZnO/Cu <sub>2</sub> O/Cu <sub>2</sub> O+	0.9	0.32	ECD	[63]
ZnO/Cu <sub>2</sub> O	0.47	0.28	ECD	[64]
ZnO/Cu <sub>2</sub> O	0.41	0.32	ECD	[65]
ZnO/Cu <sub>2</sub> O	1.46	0.49	AALD	[47]
ITO/Zn <sub>0.79</sub> Mg <sub>0.21</sub> O/Cu <sub>2</sub> O	2.2	0.65	AALD	[47]

Patent WO2019058605A1 [66] presents a multi-junction tandem solar cell with improved efficiency and a Cu<sub>2</sub>O absorbent layer. It includes: (1) a first electrode, (2) a light absorption layer, (3) an n-type layer, and (4) a second electrode. The light absorption layer is between the first electrode and the n-type layer; the n-type layer is between the light absorption layer and the second electrode.

### 3. Characterization of Cu<sub>2</sub>O and ZnO Layer Structures

#### 3.1. Characterization of Cu<sub>2</sub>O Layer Structure

##### 3.1.1. Basic Information

Cu<sub>2</sub>O is one of the most efficient metal oxides for PV applications. It is a natural p-type semiconductor with a band gap of 2.1 eV. Nitrogen doping in Cu<sub>2</sub>O would reduce resistivity and improve hole concentration [67]. Cu<sub>2</sub>O thin films were deposited on quartz and silicon substrates by d. c. MSP system [68].

The layer structure of Cu<sub>2</sub>O: N thin film samples is presented in Table 2 [42].

**Table 2.** Layer structure of Cu<sub>2</sub>O:N thin films [42].

Sample Name	Gas Flow Conditions	Grains Size (nm)
Sample 0	Ar/O <sub>2</sub> was fixed at 42.5/7.5 sccm undoped	20–90
Sample 1	(Ar/O <sub>2</sub> was fixed at 42.5/7.5 sccm) N-doped 3 sccm	20–48
Sample 2	(Ar/O <sub>2</sub> was fixed at 42.5/7.5 sccm) N-doped 1 sccm	30–54
Sample 3	(Ar was varied at 41.5 sccm, O <sub>2</sub> was fixed at 7.5 sccm)	40–88

##### 3.1.2. Morphological Characterization of the Cu<sub>2</sub>O: N Thin Films

The surface morphology of the Cu<sub>2</sub>O: N thin films could be analyzed by SEM with a scanning electron microscope, while the topographic imaging could be performed by AFM with an atomic force microscope.

###### A. Scanning Electron Microscopy (SEM)

The SEM images of four samples (see Table 2) are shown in Figure 4: one undoped Cu<sub>2</sub>O film (Sample 0) and three Cu<sub>2</sub>O: N thin film samples (Samples 1–3) [42].

###### B. Atomic Force Microscopy (AFM)

The grain size, including surface roughness of Cu<sub>2</sub>O: N thin film deposited on quartz substrate, is measured by AFM topographic imaging. The surface morphologies for each of the N-doped thin film samples compared to Sample 0 are shown: (1) in Figure 5a as 2D AFM images, together with their corresponding profile histograms, and (2) in Figure 5b as 3D AFM images. The root-mean-square surface roughness ( $R_{RMS}$ ) for each sample is extracted from their AFM images [69,70].

The histograms represent the statistical distribution of the height surface profile of the Cu<sub>2</sub>O samples derived from the AFM images. Samples 1, 2, and 3 present the highest frequency at a surface height of 26 nm, 25 nm, and 17 nm, respectively.  $R_{RMS}$  and Height

Distribution Standard Deviation are resulted from the histograms based on the 2D AFM images, processed in MATLAB, and presented in Table 3 [42].

**Table 3.** Height Distribution Standard Deviation resulted from histograms of 2D AFM images and  $R_{RMS}$  of  $Cu_2O$  thin films [42].

Sample Deposited on Quartz	$R_{RMS}$ (nm)	Height Distribution Standard Deviation (nm)
Sample 0	6.3	7.8
Sample 1	4.7	5.8
Sample 2	4.2	4.5
Sample 3	3.9	4.2

The undoped  $Cu_2O$  film (Sample 0) presents a greater roughness than the doped Samples 1–3. Sample 1 presents the highest deviation and Sample 3 has the lowest one using the doped samples.

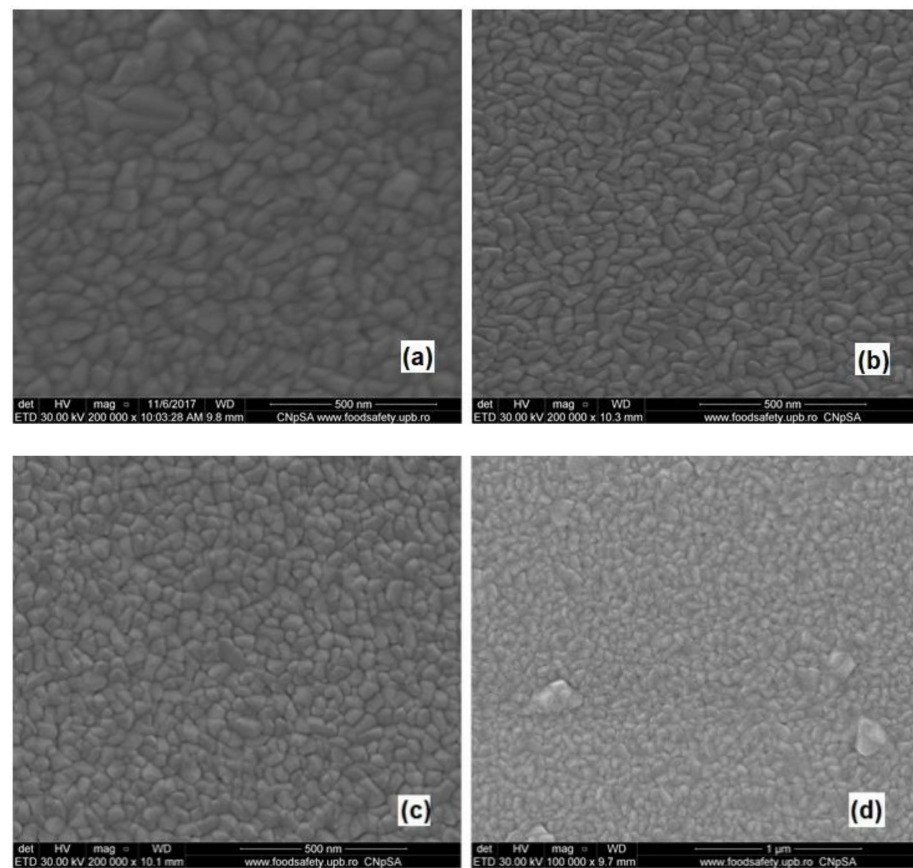
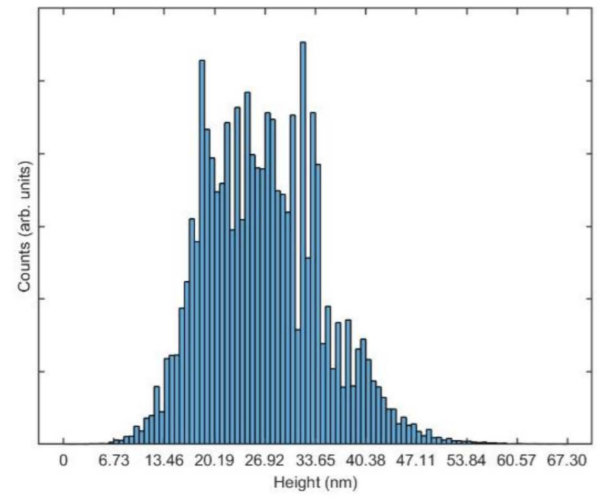
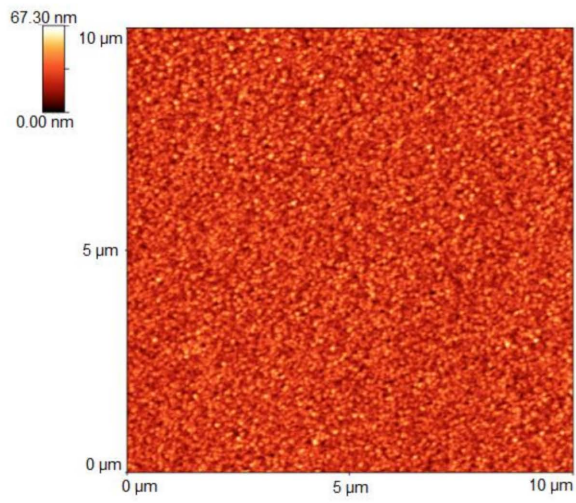
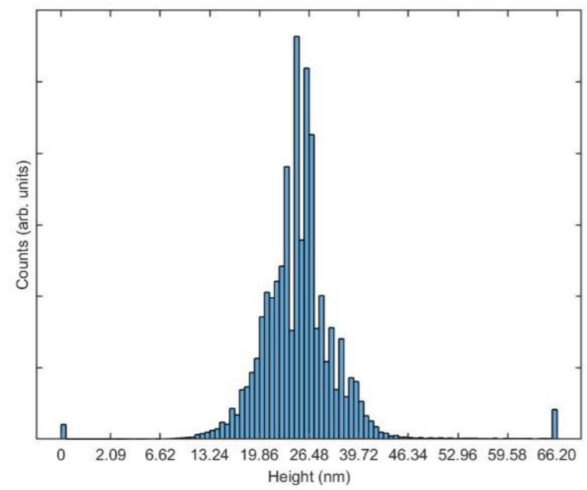
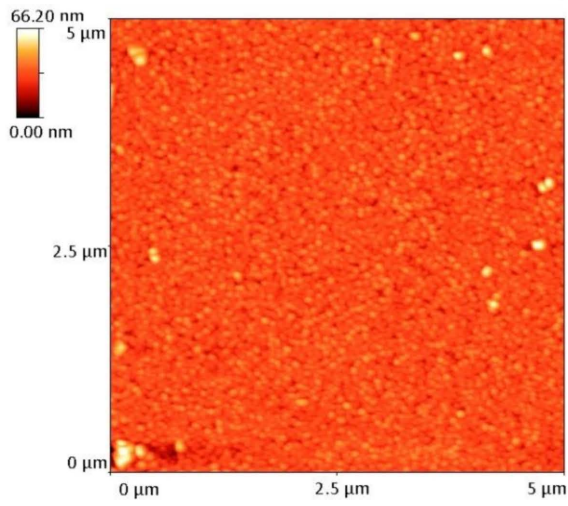


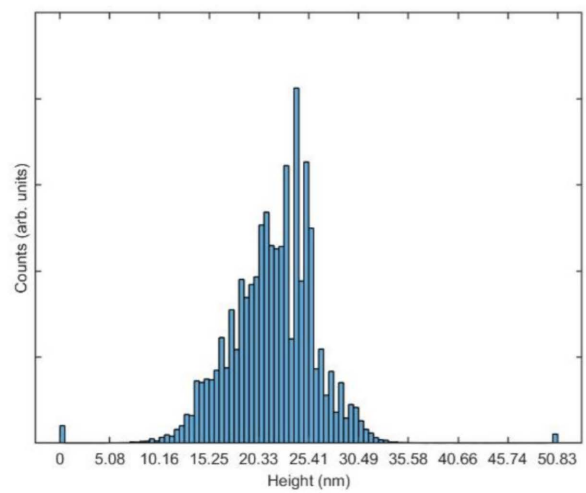
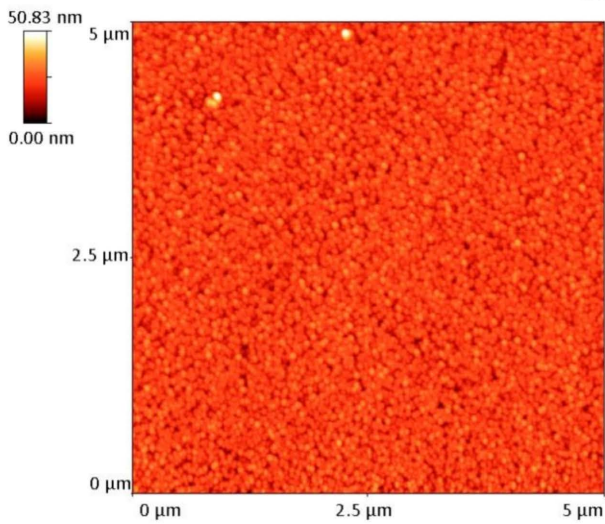
**Figure 4.** SEM images of  $Cu_2O$  thin films deposited on quartz substrate: (a) Sample 0, (b) Sample 1, (c) Sample 2, and (d) Sample 3 [42].



Sample 0



Sample 1



Sample 2

Figure 5. Cont.

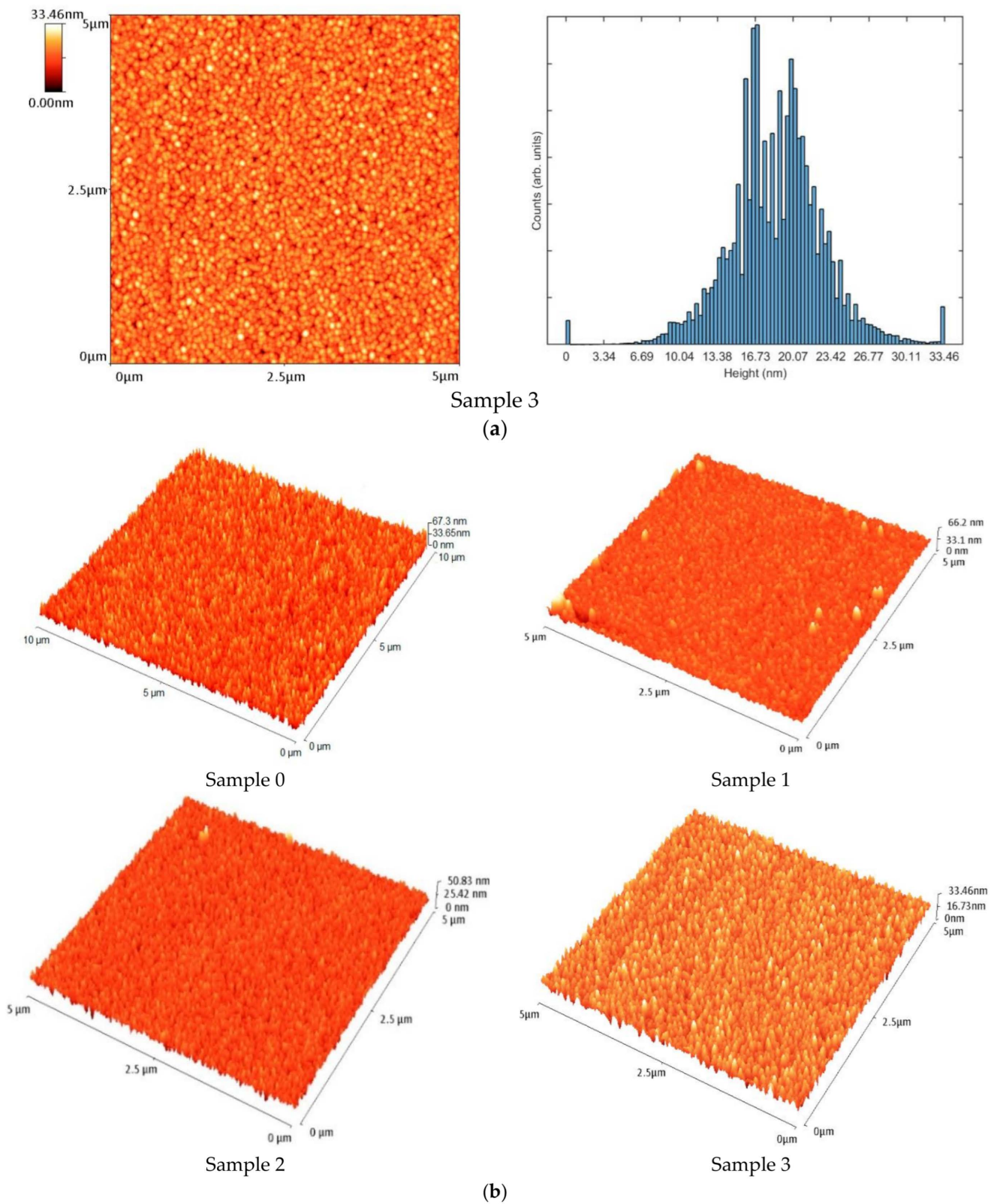


**Figure 5.** (a) 2D AFM images of Samples 0–3 and their corresponding histograms [67]; (b) 3D AFM images of Samples 0–3 [42].

### 3.1.3. Structural Characterization by XRD of the Cu<sub>2</sub>O:N Thin Films

The XRD patterns of the four samples recorded in the range 30–60° were obtained by a diffractometer (see Figure 6); all films are dominated by two reflection peaks. The XRD patterns are not significantly influenced by nitrogen doping [53].

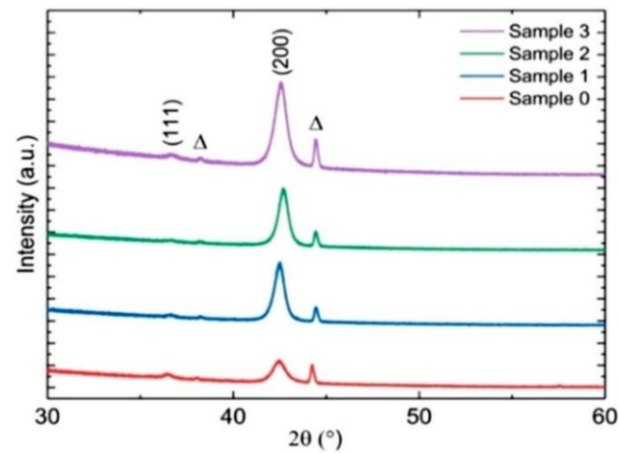


**Figure 6.** XRD patterns of Samples 0–3 in the range 30–60°, where  $\Delta$  represents the background peak [42].

The Cu<sub>2</sub>O peaks are determined by comparing experimental XRD peak patterns with the ICDD patterns (standard Powder Diffraction cards) [71,72].

### 3.1.4. Optical Characterization of the Cu<sub>2</sub>O:N Thin Films

Optical characterization is carried out by (1) *FTIR spectroscopy* analysis using a Perkin–Elmer spectrometer, and (2) *spectroscopic ellipsometry (SE)* using a spectroscopic ellipsometer. The refractive index and extinction coefficient of Cu<sub>2</sub>O: N thin films in the range from 190 to 2100 nm could be determined based on SE.

#### A. FTIR Spectroscopy characterization.

Figure 7 shows the FTIR transmission spectra obtained for Cu<sub>2</sub>O: N thin films. Table 4 lists the transmission peaks [42].

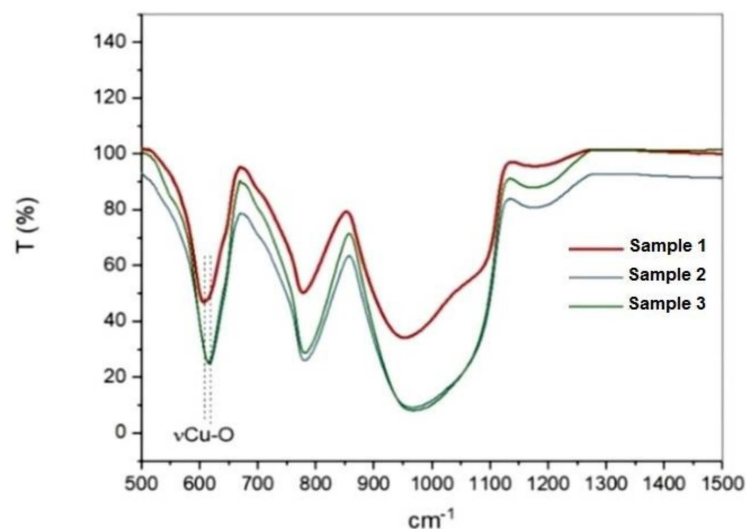


**Figure 7.** FTIR transmission spectra for Cu<sub>2</sub>O:N thin film: Sample 1, Sample 2, and Sample 3 [42].

**Table 4.** Transmission peaks for Cu<sub>2</sub>O: N thin films [42].

Sample Name	$\nu$ Cu <sub>2</sub> O (cm <sup>-1</sup> )
Sample 1	608
Sample 2	616
Sample 3	615

The FTIR spectra of all samples deposited on quartz show the peaks corresponding to the vibrational modes of Si-O that belong to the quartz substrate [72,73]. An increasing trend is remarked in the intensity of the Cu<sub>2</sub>O:N absorption band from Sample 1 to Sample 3, determining an increased concentration of N<sub>2</sub>, in good agreement with the recent predictions [74]. The decrease in resistivity and increase in N-doping concentration is explained by annealing-driven substitution of O atoms with implanted N atoms; N doping may induce any variation in energy band structure of Cu<sub>2</sub>O films [71]. The photoluminescence (PL) spectra of Cu<sub>2</sub>O films contain two main signals ranging from 450 to 650 nm [75].

#### B. Spectroscopic Ellipsometry (SE) Characterization

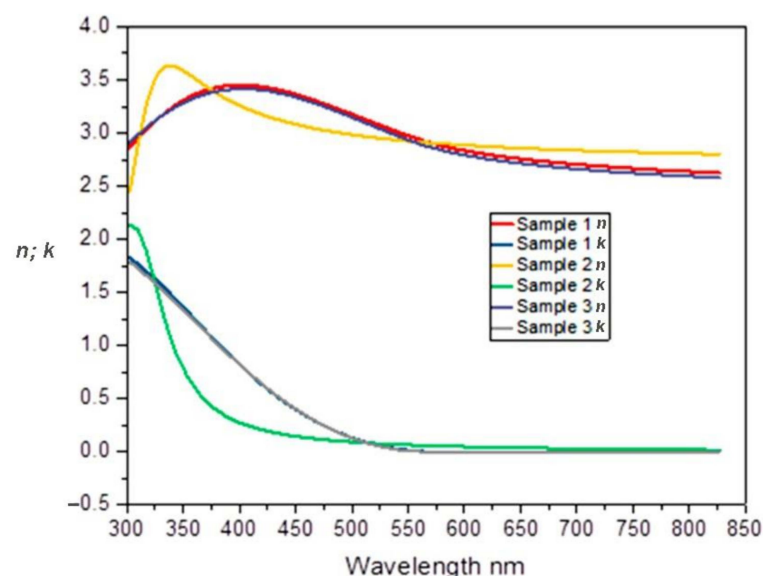
The investigated spectroscopic ellipsometry (SE) parameters of Cu<sub>2</sub>O:N thin films in the range 1.5–4.1 eV are (1) the band gap, and (2) the surface roughness [76,77], see Table 5.

**Table 5.** Investigated (SE) parameters of Cu<sub>2</sub>O:N thin films [76,77].

Sample Name	Sample 1	Sample 2	Sample 3
Band gap (eV):	2.17	2.14	2.17
Surface roughness (nm):	15.9	19.6	17.2

Using the Tauc–Lorentz oscillator modelling [78], the following parameters can be determined: (1) the band gap, (2) the surface roughness, (3) the refractive index ( $n$ ), and (4) the extinction coefficient ( $k$ ) in the range 300–800 nm (from VIS to near IR) for Cu<sub>2</sub>O thin films deposited on quartz substrates.

The surface roughness of Cu<sub>2</sub>O films increases with the level of N<sub>2</sub> pressure (see Table 5). The presence of N<sub>2</sub> during deposition of Cu<sub>2</sub>O films on quartz substrate produces small changes over  $n$  and  $k$  in the range 300–600 nm for Samples 1–3, see Figure 8.

**Figure 8.** Graphs of  $n$  and  $k$  coefficients for Samples 1, 2, and 3 of Cu<sub>2</sub>O:N thin films;  $\lambda$  is wavelength [67].

In Figure 8 for Sample 2 (the highest N-doped sample), the changes in  $n(\lambda)$  (yellow curve) and  $k(\lambda)$  (green curve) associated with a structural change in  $\text{Cu}_2\text{O}$  induced by nitrogen doping could be seen. This could be a promising method for modifying the optical properties of the metal oxide [75,79]. The crystal size decreases with the increasing of the N-doping concentration in the small N-doping range [72,75].

### 3.2. Characterization of ZnO Layer Structure

#### 3.2.1. The Structural Properties of ZnO Nanostructures

For bulk ZnO, structural characterization by X-ray diffraction (Figure 9a) reveals peaks belonging to Zn [80], up to 500 °C; at 700 °C, small peaks of ZnO would appear [81]. For the non-annealed ZnO thin film, the X-ray diffraction patterns (Figure 9b) show four peaks that belong to Zn and are compatible with the crystal structure [82,83]. Up to 900 °C, the structure of ZnO thin films is hexagonal; at 1100 °C, the defects change the structure to a cubic one and the peaks in the X-ray spectrum shift. X-ray diffraction gives information about the crystalline and structural properties of thin films such as: lattice constants, particle size, displacement density, and microcontroller [84].

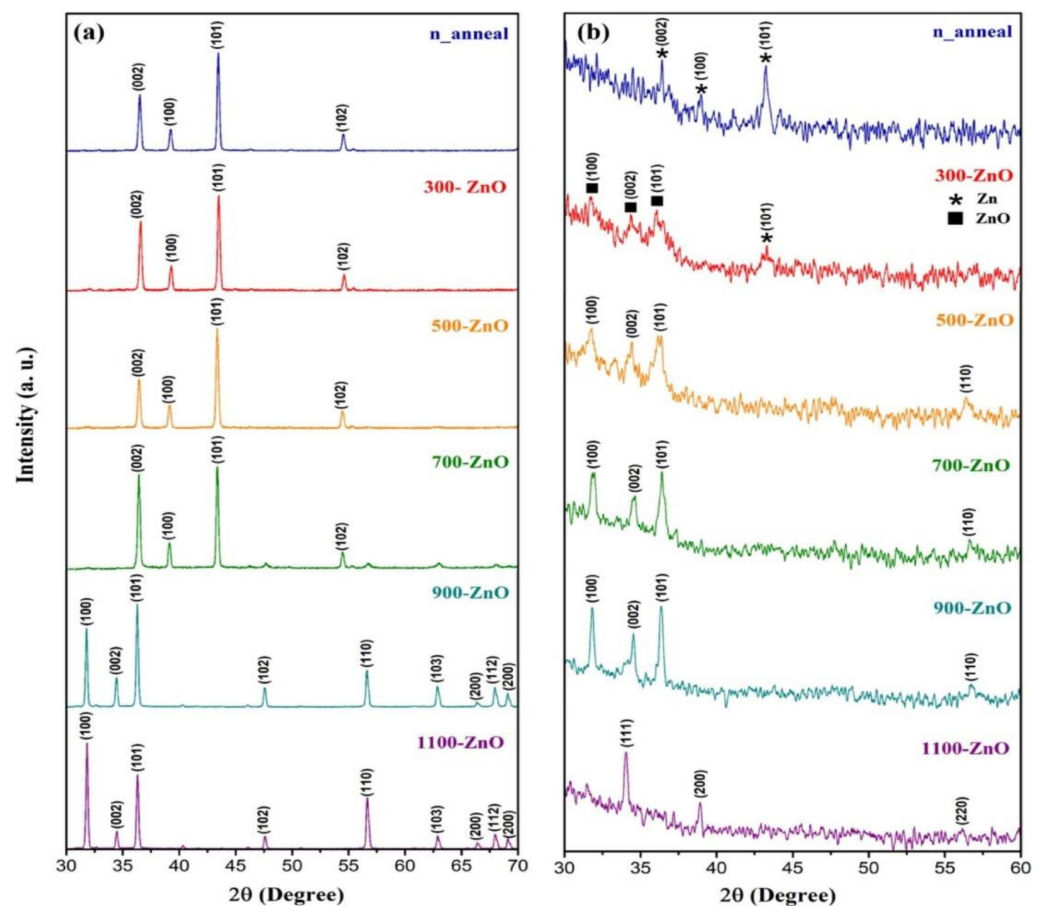


**Figure 9.** XRD patterns of Zn and ZnO bulk samples: (a) thin films [80]; (b) annealed at different temperatures [82].

The best ways to study ZnO morphology are (1) the size; (2) the shape; and (3) the placement of particles on the body surface [85]. For the thin films, it shows that the synthesized nanoparticles are spherical and uniform in size (Figure 10a); by increasing the temperature, the oxidation of the films and the size of the crystalline grains decrease. The AFM images of the samples (Figure 10b) show that the surface morphology changes as the temperature increases; the surface roughness and average surface height increase. Different

properties of bulk samples and thin films, such as roughness and surface morphology, depend on their crystal structure.

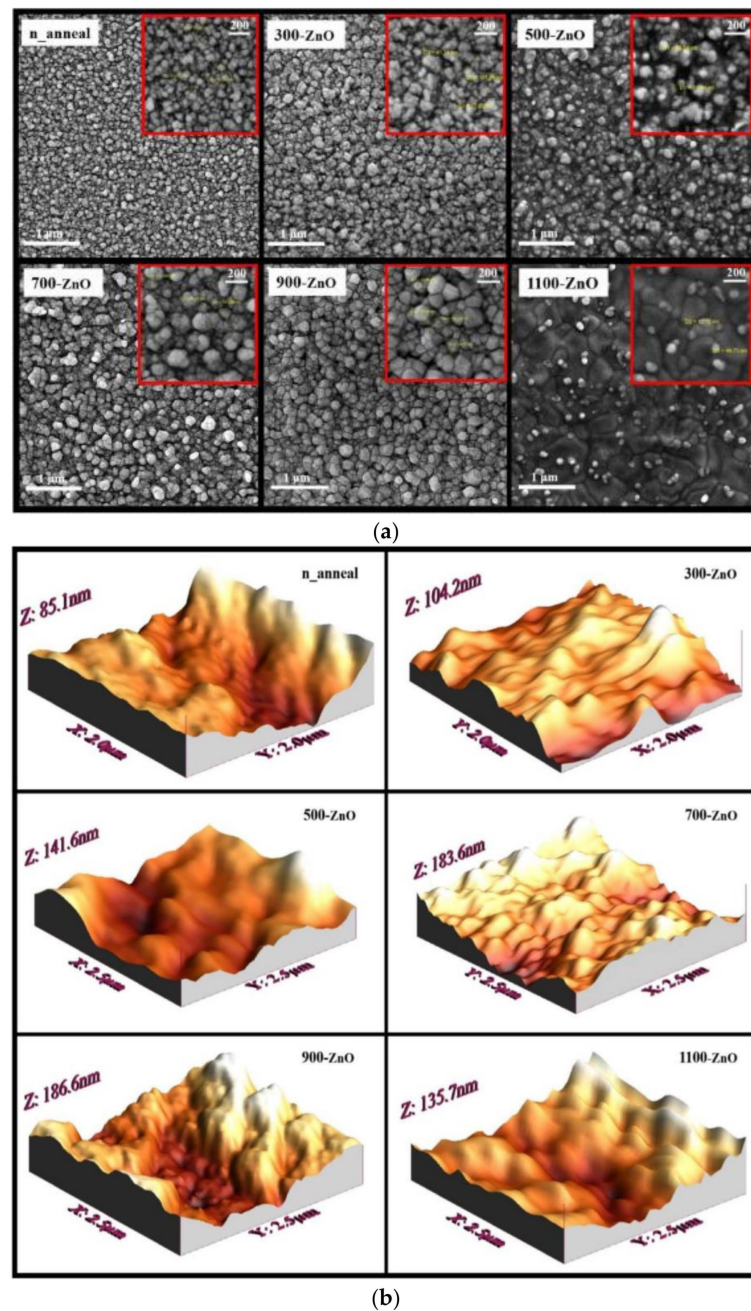


**Figure 10.** (a) SEM images of Zn and ZnO thin films annealed at the temperatures of 300, 500, 700, 900, and 1100 °C [85]. (b) AFM images of Zn and ZnO thin films annealed at different temperatures [46].

### 3.2.2. Optical Properties of ZnO Thin Films

#### A. UV-VIS Spectroscopy

The effects of annealing temperature on the optical properties of ZnO thin films, namely absorbance and transmittance in VIS and UV, are investigated. The UV absorbance increases due to the increase in the annealing temperature and the spectrum shifting towards shorter wavelengths (Figure 11a); it is obtained by the decrease of the particle size and the increase of the energy bandgap. The transmittance is strongly affected by the annealing temperature and increases sharply in the VIS. Also, in the UV, the transmittance (Figure 11b) decreases to a minimum; a strong interaction is indicated between the incident

light and the material electrons; light scattering is caused and particle size increases grain area as well as reduced light transmission.

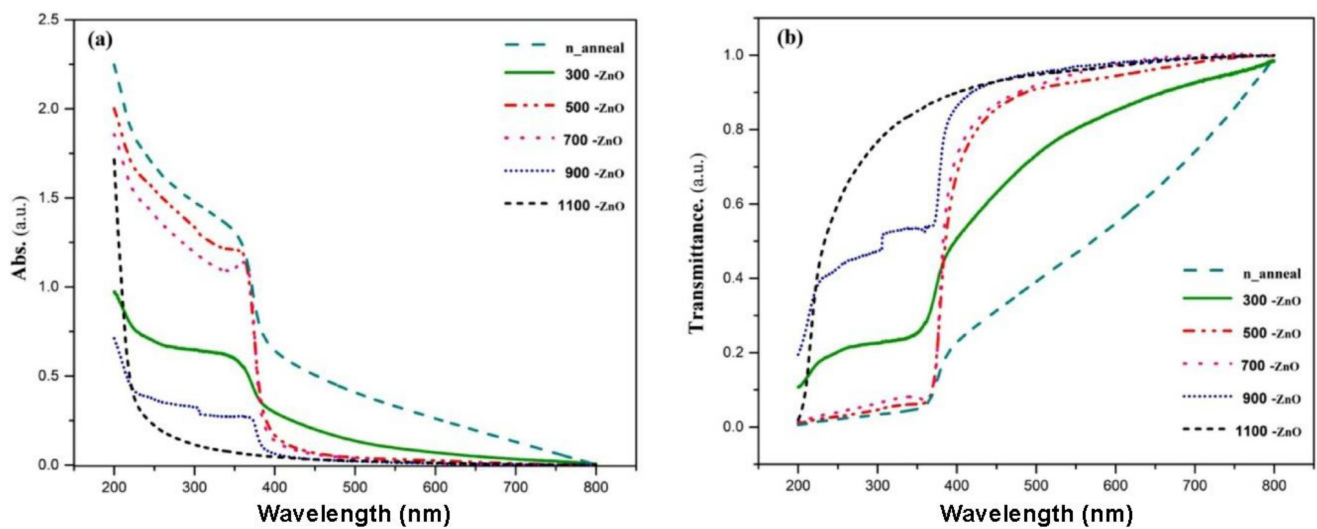


**Figure 11.** The absorption (a) and transmittance (b) spectra of the prepared thin films [86].

### B. Photoluminescence (PL) Spectroscopy

Photoluminescence (PL) and UV–VIS absorption measurements can be performed at room temperature. The PL spectrum shows that the relative intensity of UV and defect bands depends on the length of ZnO nanorods. The peak of PL of UV band around 395 nm is strongly enhanced when the length of ZnO nanorods is reduced. PL spectrum of ZnO nanostructures is defined by emission bands observed in UV and VIS. The UV peak is a characteristic of ZnO emission, and the VIS light emission density is much higher [87]. For PL spectroscopy, the intensity of UV peaks increases by increasing of the annealing temperature (Figure 12); the intensity of peaks in VIS is low and strong exciton emission indicates that ZnO nanoparticles have a minor defect.

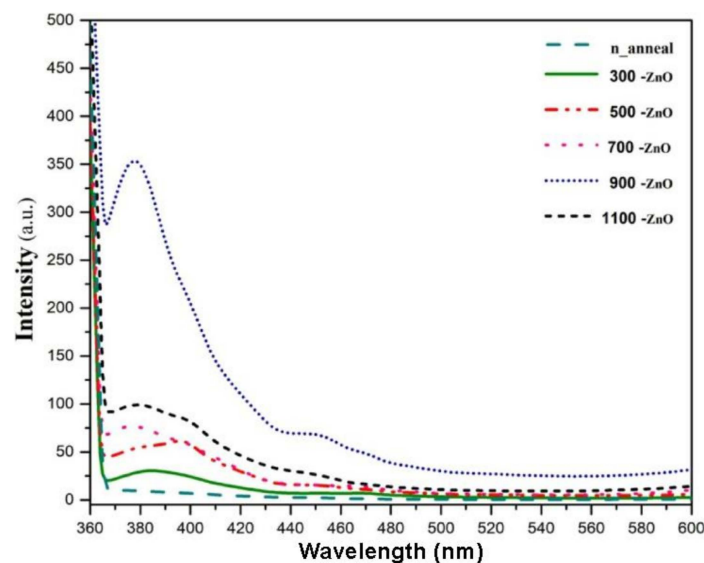


**Figure 12.** PL spectroscopy of Zn and ZnO nanostructured thin films [83].

### C. Determination of Optical Constants

High transparency of transmittance over the VIS makes it possible for ZnO to be used in solar cells. It is essential to know the optical parameters of thin films, especially

the refractive index and extinction coefficient [86]. Figure 13 proves the following graphs: (1) extinction coefficient, (2) refractive index, and (3) real and imaginary parts of the complex dielectric function of prepared thin films. The extinction coefficient is the lowest for ZnO and the highest for n-anneal in VIS. Refractive index decreases in the transparent region (long wavelengths) and increases in the absorption region (short wavelengths). Real and imaginary parts of the dielectric function feature a decreasing trend in the transparent region. The absorption area expands toward shorter wavelengths. The extinction coefficient, refractive index, and real and imaginary parts of the dielectric function enhance in tandem with the increasing of the annealing temperature, up to 900 °C. The optical conductivity of nanoparticles is presented in terms of the landing photon energy (Figure 14). Higher values of optical conductivity indicate that the grown ZnO thin film has high potential to be used as an optically conducting material [88].

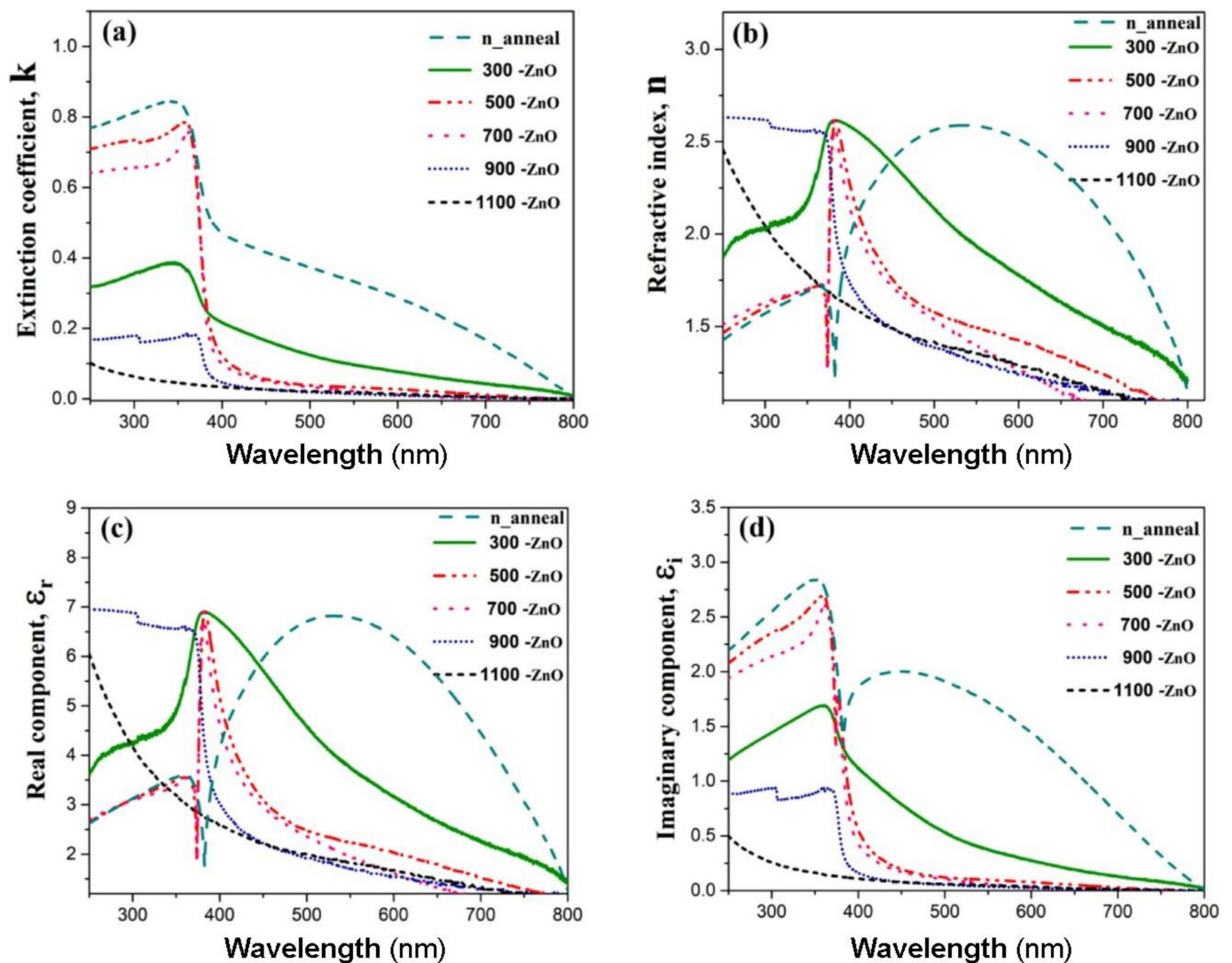


**Figure 13.** The extinction coefficient (a) refractive index (b) and real (c) and imaginary (d) portions of complex dielectric function of the thin films [86].

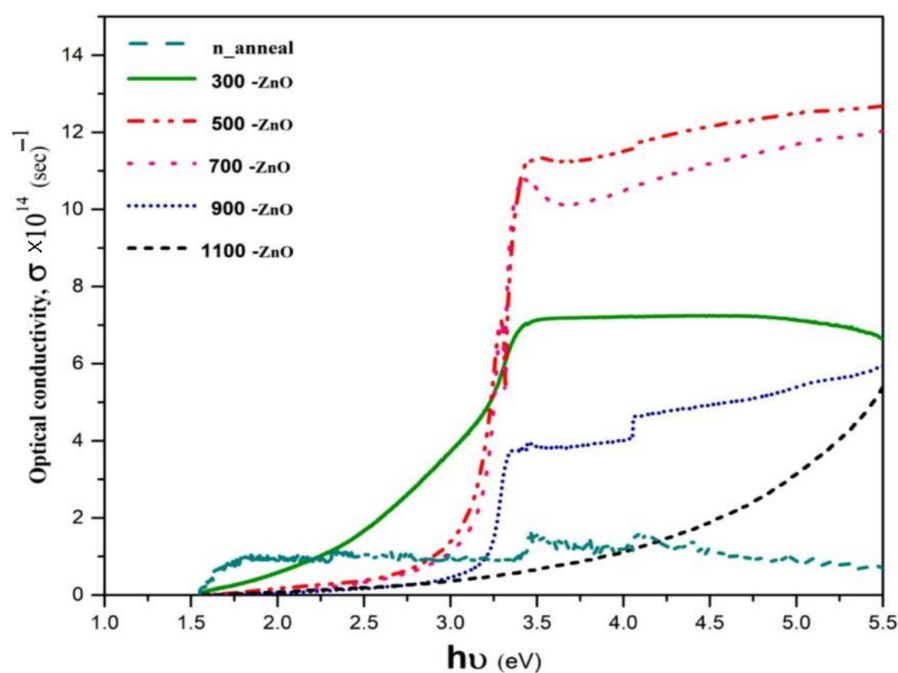


**Figure 14.** Optical conductivity of the prepared nanoparticles in terms of energy of landing photon [88].

#### 4. Merits and Comparative Analysis of AZO/Cu<sub>2</sub>O HTSC

##### 4.1. Merits of AZO/Cu<sub>2</sub>O Heterojunction Tandem Solar Cells (HTSC)

The highest experimental efficiency of ZnO/Cu<sub>2</sub>O HTSC determined so far is 5.38%, see Minami et al. [52], by depositing firstly a Ga<sub>2</sub>O<sub>3</sub> buffer layer and secondly an AZO layer by PLD on Cu<sub>2</sub>O layer. This is far from the theoretical conversion efficiencies of Cu<sub>2</sub>O and ZnO, which are 20% and 18%, respectively. The most prominent challenges that are identified are tied to the material quality of the Cu<sub>2</sub>O layer, namely high resistivity and low crystallinity, as a result of Cu<sub>2</sub>O contamination at the surface. The surface defects on the Cu<sub>2</sub>O lead to unwanted charge transport and recombination at the heterojunction interface. These challenges can be mitigated by growing crystal Cu<sub>2</sub>O, both to decrease interface defects, and to increase conductivity.

##### 4.2. Comparative Analysis of HTSC with Other High Performance Solar Cells

A comparative analysis of efficiencies and device characteristics for solar cells with the highest certified efficiency to date concerning: DSSCs, PSCs, OPVs, and Tandem PSCs (HTSC) is discussed based on the data in Table 6 [89]. Advanced techniques and research trends can be examined from the perspective of (1) novel materials, (2) device modelling, and (3) innovative device structures. The comparative advantages and limitations of these photovoltaic technologies are evaluated in terms of (1) device efficiency, (2) durability, (3) ease of fabrication, and (4) performance–price ratio.

**Table 6.** Highest recorded efficiencies and device characteristics for DSSCs, PSCs, OPVs, and HTSCs [89].

	Efficiency (%)	Active Layer/Absorber	Carrier Transporting Material	Innovative Materials/Techniques	Institution/Company
DSSC	13.0	TiO <sub>2</sub> dye-sensitized semiconductor	Cobalt redox couple electrolyte	Panchromatic porphyrin sensitizers	EPFL
PSC	25.2	FAPbI 3-based perovskite	Spiro-MeOTAD	Minimizing the deformation of photoactive layers by changing the type and ratio of ions	UNIST

Table 6. Cont.

	Efficiency (%)	Active Layer/Absorber	Carrier Transporting Material	Innovative Materials/Techniques	Institution/Company
Tandem PSC/Si	29.5	Monolithic perov-skite PbI <sub>2</sub> -based top cell/Si bottom cell	Methyl-substituted carbazole monolayer/C <sub>60</sub>	Self-assembled carbazole-based monolayer with methyl group substitution	Oxford PV
Tandem PSC/CIQS	24.2	Monolithic two-terminal triple-cation PSC/CIQS	Poly [bis(4-phenyl) (2,4,6-trimethylphenyl) amine] (PTAA)/C <sub>60</sub>	Rubidium-based self-assembled monolayer	HZB
OPV	18.2	PBDB-T-2F:BTP-eC9	PEDOT:PSS	Chlorinated nonfullerene acceptor	SJTU/BUAA

## 5. Numerical Modelling of Heterojunction Tandem Cu<sub>2</sub>O/ZnO Solar Cells

### 5.1. Multiscale Modelling of PV Technology

The computational modelling approach of PV technology is developed based on the following items: (1) material properties; (2) nanoscale structures defined by dynamical electronic, thermal, and optical properties, and interface processes that determine mesoscale methods; (3) solar PV devices (solar cells); and (4) industrial applications represented by PV systems. The analysis of nanoscale structures based on electronic, thermal, and optical properties together with their influence on solar cells' characteristics involves a *multiscale modelling* (defined by: *atomic scale, mesoscale, μm and cm to meter scale*), and *characterization*, see Figure 15 [90–92]. In the following paragraphs of this section, the analyzed solar cell (μm scale), respectively, the Heterojunction Tandem Cu<sub>2</sub>O/ZnO solar device, is discussed based on numerical modelling.

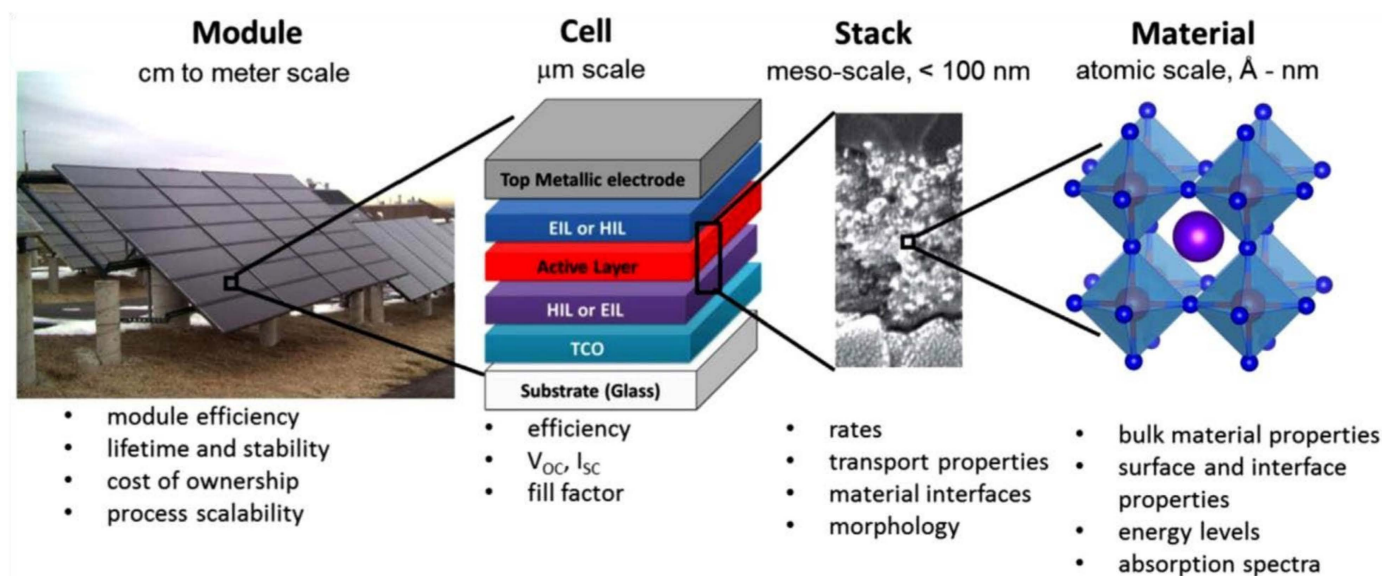


Figure 15. Interesting scales in photovoltaics technology and corresponding quantities [90–92].

### 5.2. Diagram of the Cu<sub>2</sub>O/ZnO Solar Cell Simulation Model

A diagram of the simulated model for Cu<sub>2</sub>O/AZO tandem heterojunction solar cell is represented in Figure 16. This solar cell structure includes (1) a quartz glass superstrate; (2) an AZO n+ emitter layer; (3) a Cu<sub>2</sub>O p-type absorber layer; and (4) a bottom Cu<sub>2</sub>O: N layer.



**Figure 16.** Diagram of the simulated Cu<sub>2</sub>O/AZO solar cell [28].

### 5.3. Simulation Methodology

Numerical modelling of the Cu<sub>2</sub>O/ZnO(AZO) can be studied based on three simulation software packages, namely Silvaco Atlas, MATLAB, and Quokka 2. The simulated solar cell is analyzed for two sub-cells: (1) Cu<sub>2</sub>O/ZnO(AZO) top sub-cell; (2) c-Si bottom sub-cell.

The best simulators used for solar cell design and material performance optimization are *Silvaco Atlas* and *PC1D*. Silvaco is an efficient tool for the top sub-cell and absorbs the high solar energy part while PC1D is an optimum tool for the bottom sub-cell and absorbs the low solar energy part. The simulated device with optimized parameters can be compared with the experimental industrial metal oxide solar cell; based on this comparison, the validation can be done.

The large current mismatch between the two sub-cells, caused by the large band gap difference for the two absorbers, allows the optimization of the top and bottom sub-cells and defines the arrangement of a four-terminal configuration. This approach can increase the conversion efficiency of the tandem heterojunction ZnO/Cu<sub>2</sub>O silicone solar cell beyond the limit of the conventional c-Si solar cell.

A 4T tandem SC can be connected to two loads such that each sub-cell always operates at its maximum power point (MPPT). This MPPT maximizes energy production and requires additional current collection which would decrease performance. An idealized 4T tandem SC with no resistive or optical losses serves as an upper limit for performance. 4T SC must also be designed to operate such that the top and bottom sub-cells are electrically isolated, which may introduce additional optical losses and series resistances.

The excellent performance of idealized 4T tandem SCs and current-matched 2T tandem SCs is highlighted. Similar trends are seen for both the energy-harvesting efficiency under a set of spectra, and power-conversion efficiency under the AM1.5G spectrum. This analysis can be extended to different locations with different climates, and different sub-cell materials.

### 5.4. Electrical Numerical Modelling for the Two Sub-Cells of the HTSC

#### 5.4.1. Electrical Modelling of the Top Sub-Cell

This numerical modelling is investigated using the Silvaco Atlas simulation package. The ZnO(AZO) is selected as the *buffer layer*; a buffer layer is required in a material system to obtain a large enough conduction band offset. The influence of defects [18,48,93–96] is discussed taking into account that an interface defect layer (IDL) is implemented.

Based on simulations, the following graphs are obtained: (1) the dependence of the AZO thickness on top sub-cell efficiency with an optimum AZO thickness of 0.25 μm, see Figure 17a; (2) the dependence of IDL thickness on top sub-cell efficiency ( $\eta$ ), see Figure 17b; (3) the dependences of buffer electron mobility on top sub-cell fill factor (FF) and conversion efficiency ( $\eta$ ), see Figure 17c; (4) the dependence of buffer and IDL affinity on top sub-cell efficiency ( $\eta$ ), see Figure 17d.

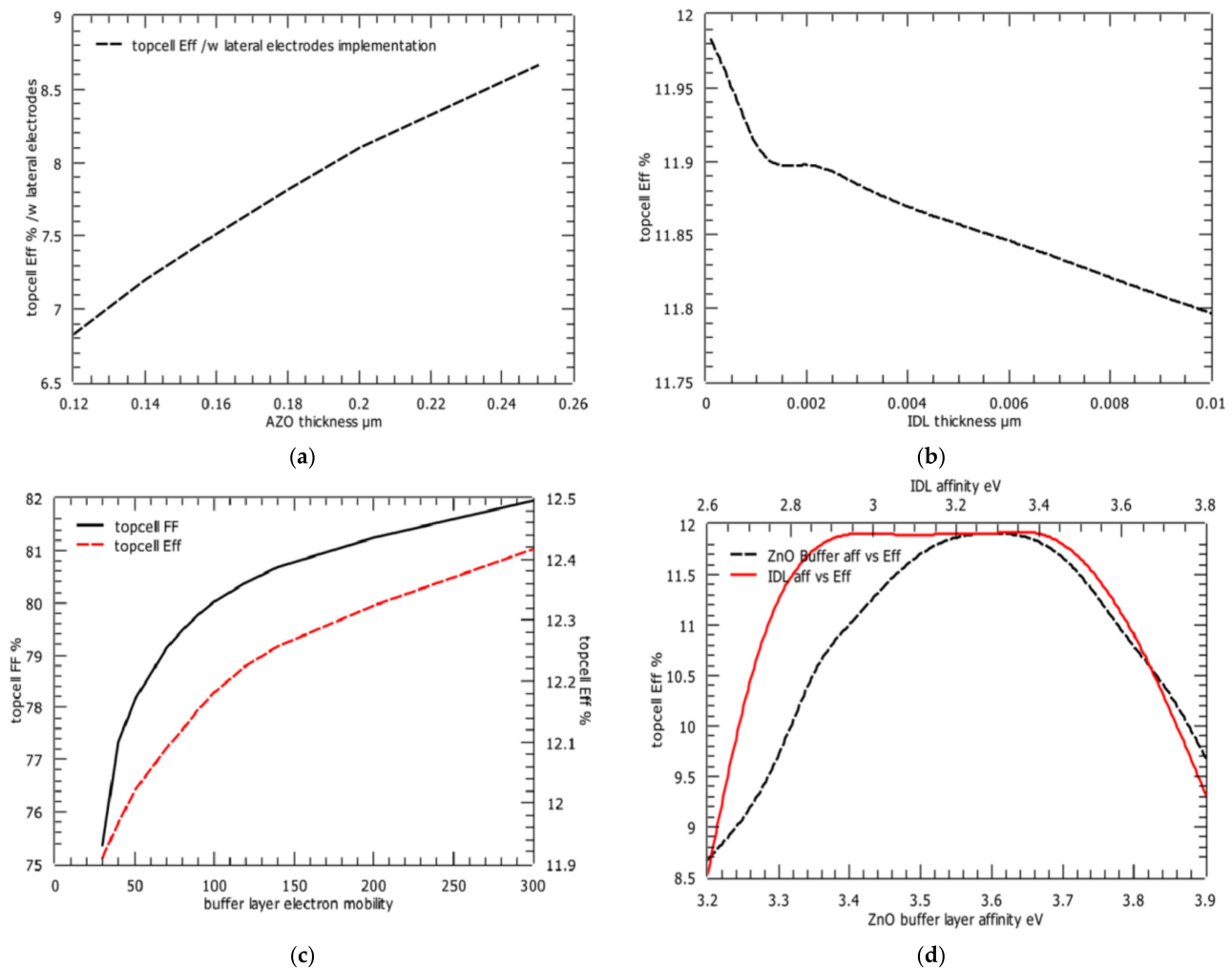


**Figure 17.** (a) AZO (Al: ZnO) thickness vs. top sub-cell efficiency; (b) interface defect layer (IDL) thickness vs. top sub-cell efficiency [93]; (c) buffer electron mobility ( $\text{cm}^2/\text{V}\cdot\text{s}$ ) vs. top sub-cell fill factor and conversion efficiency; (d) buffer and IDL affinity vs. top sub-cell efficiency [93].

The following is remarked:

- a buffer electron mobility value under  $100 \text{ cm}^2/\text{V}\cdot\text{s}$  would influence FF and  $\eta$ ;
- a comparison of different buffer and IDL materials can be done from the point of view of their affinity. The optimal affinity interval for the buffer layer is 3.4–3.6 eV; it would define the lower conduction band offset with  $\text{Cu}_2\text{O}$  absorber layer. The optimal affinity interval for IDL is 2.95–3.4 eV.

#### 5.4.2. Electrical Modelling of the Bottom Sub-Cell

This electrical modelling is studied based on the Quokka 2 software, version 2.2.5. The experimental results can be compared with the simulated ones. The J-V characteristics, experimental curve and simulated one, respectively, are presented in Figure 18a. At the same time, the experimental and simulated graphs of the external quantum efficiency (EQE) are plotted in Figure 18b.

The essential electrical parameters for the bottom (c-Si) solar sub-cell are obtained using the fitting of the experimental curve with the Quokka 2 simulated one; they can be used for control and prediction. In Table 7 four experimental electrical parameters for the bottom silicone solar sub-cell are presented.

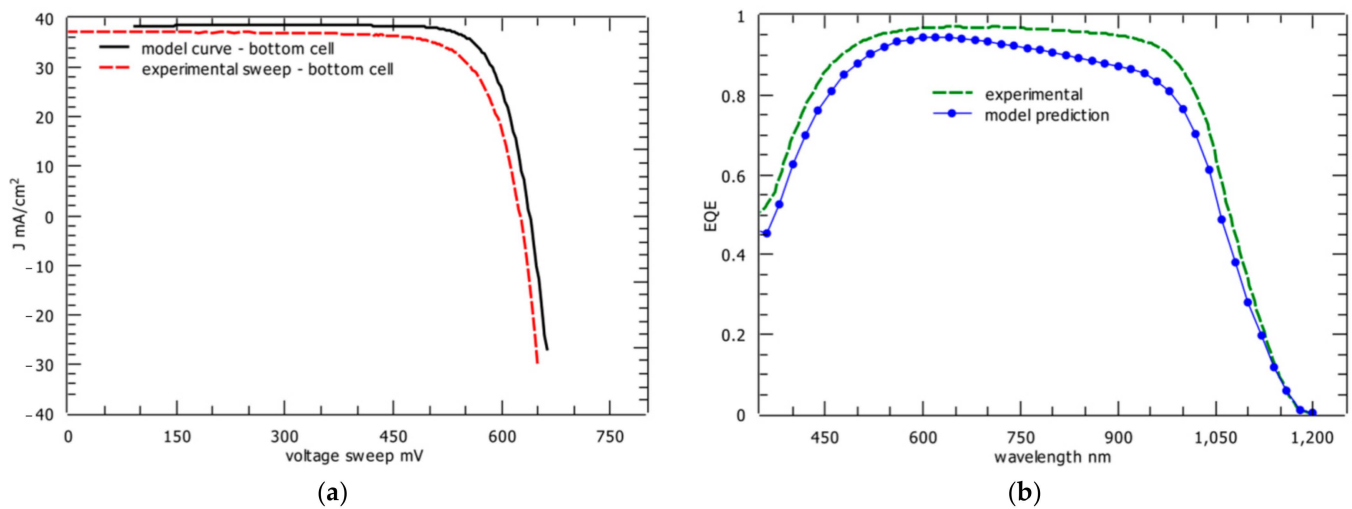


**Figure 18.** (a) Experimental vs. Quokka 2 simulated J-V curve; (b) experimental vs. Quokka 2 simulated EQE curve [28].

**Table 7.** Experimental electrical parameters for the bottom (c-Si) solar sub-cell [28].

Parameter Name	Parameter Value
Open circuit voltage, $V_{OC}$ (mV)	625.16
Fill Factor, FF (%)	76.83
Series resistance, $R_S$ ( $\text{ohm}/\text{cm}^2$ ):	0.196
Shunt resistance, $R_{SH}$ ( $\text{ohm}/\text{cm}^2$ ):	2382.8

### 5.5. Optical Numerical Modelling for the Top Sub-Cell of the HTSC

Optical characteristics for the top sub-cell, namely the reflectance, transmittance, and absorbance as function of wavelength for three samples of  $\text{Cu}_2\text{O}:\text{N}$ , can be obtained using OPAL 2 software [97–99]. The optical numerical modelling is performed in the wavelength range (300–800) nm, see Figure 19. For simulations there are implemented in the model: a 100 nm thick ZnO layer, a 2  $\mu\text{m}$  thick  $\text{Cu}_2\text{O}$  layer, and a 50 nm thick  $\text{Cu}_2\text{O}:\text{N}$  layer. The simulated reflectance would be very useful for the evaluation of loss reflectance.

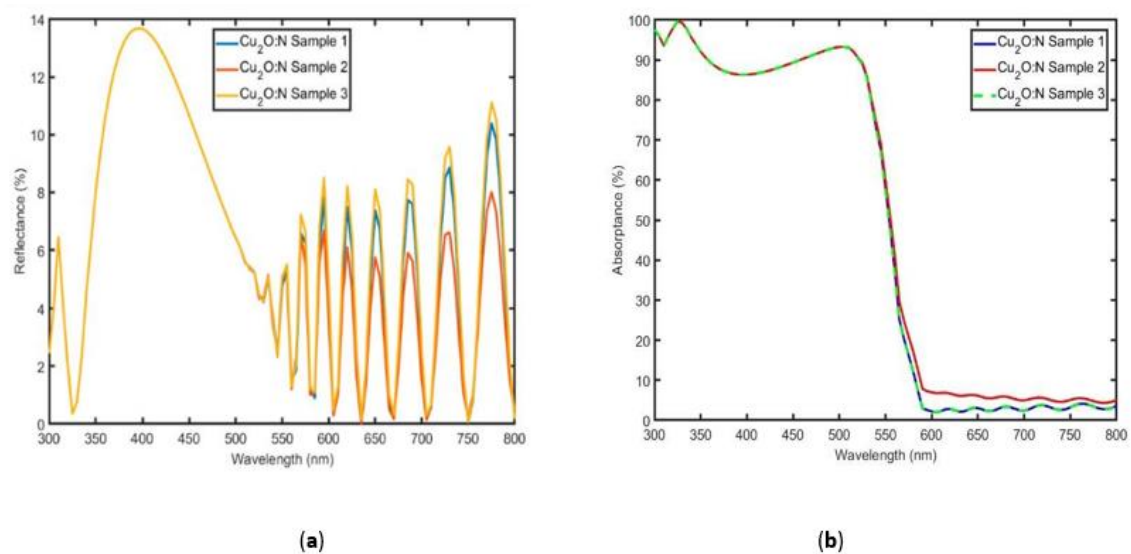


**Figure 19.** Cont.

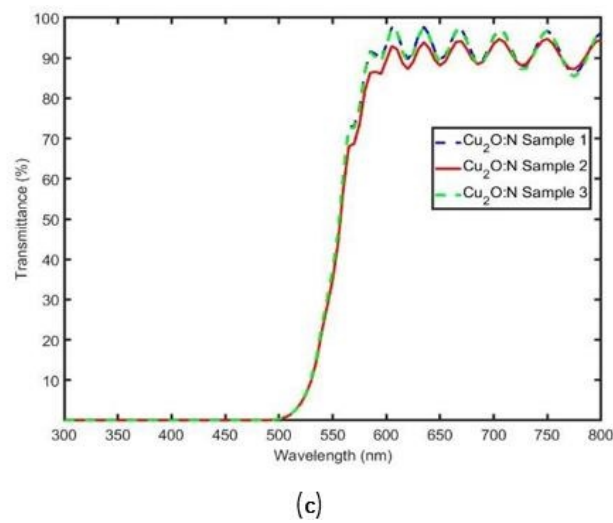


**Figure 19.** (a) Reflectance, (b) absorbance, and (c) transmittance as a function of wavelength for the metal oxide structure [100].

Based on the transmittance data, Tauc plots [100] for the three doped samples are estimated and presented in Figure 20. Tauc plots indicate an optical bandgap around 2.18 eV for all samples, in good agreement with the ellipsometry measurements (see Section 3).

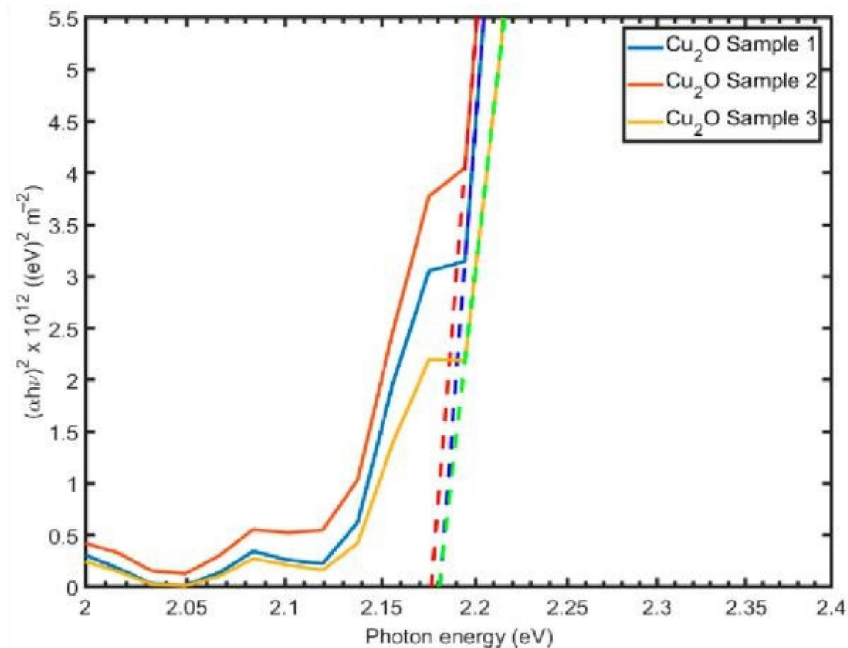


**Figure 20.** Tauc plots of Samples 1, 2, and 3 deposited on quartz substrate [100].

## 6. Stability and Reliability Approach

### 6.1. Stability Aspects

The stability is an essential parameter of commercial HTSC and can improve its lifetime. The solar cell stability would require minimizing the influence of humidity, UV, and temperature effects.

The 55% humidity can diminish the solar cell performance by color change [101]. The moisture sensitivity of solar devices can be improved by suitable encapsulation techniques. The thermal stability of HTSC would be increased by use of polymers [102]. The research regarding the rain effect with water of variable pH based on the simulation with lead poisoning participation would allow consideration of safe solar cell use [103].

### 6.2. Methodological Tools for HTSC Reliability

There are three main accelerated tests to be considered for the reliability of a solar cell:

(a) Qualitative accelerated test: it is used for information regarding the HTSC failure ways;

(b) High Accelerated Life Test (HALT): it is used for information regarding the HTSC failure mechanism and lifetime;

(c) High Accelerated Stress Screening (HASS): it is used for information regarding the HTSC operating time and failure rate within the working temperature range.

A precise reliability analysis of HTSC could be done with the SYNTHESIS simulation package [100]. The following essential tools are used: (1) *the Weibull++ tool*, which allows the lifetime analysis; (2) *the ALTA tool*, which allows the analysis of accelerated life tests and degradation degree.

### 6.3. HTSC Thermal Stability Characteristics

Three main parameters can be discussed using the Weibull statistical repartition approach [104]: (1) *the solar cell lifetime* in different conditions; (2) *the degradation degree* influenced by temperature; and (3) *the number of defects (failures)*.

The Weibull statistical repartition can be used for prediction of two essential parameters: solar cell lifetime (Figure 21a) and solar cell degradation degree based on temperature influence [105–107] under standard and stress conditions (Figure 21b).

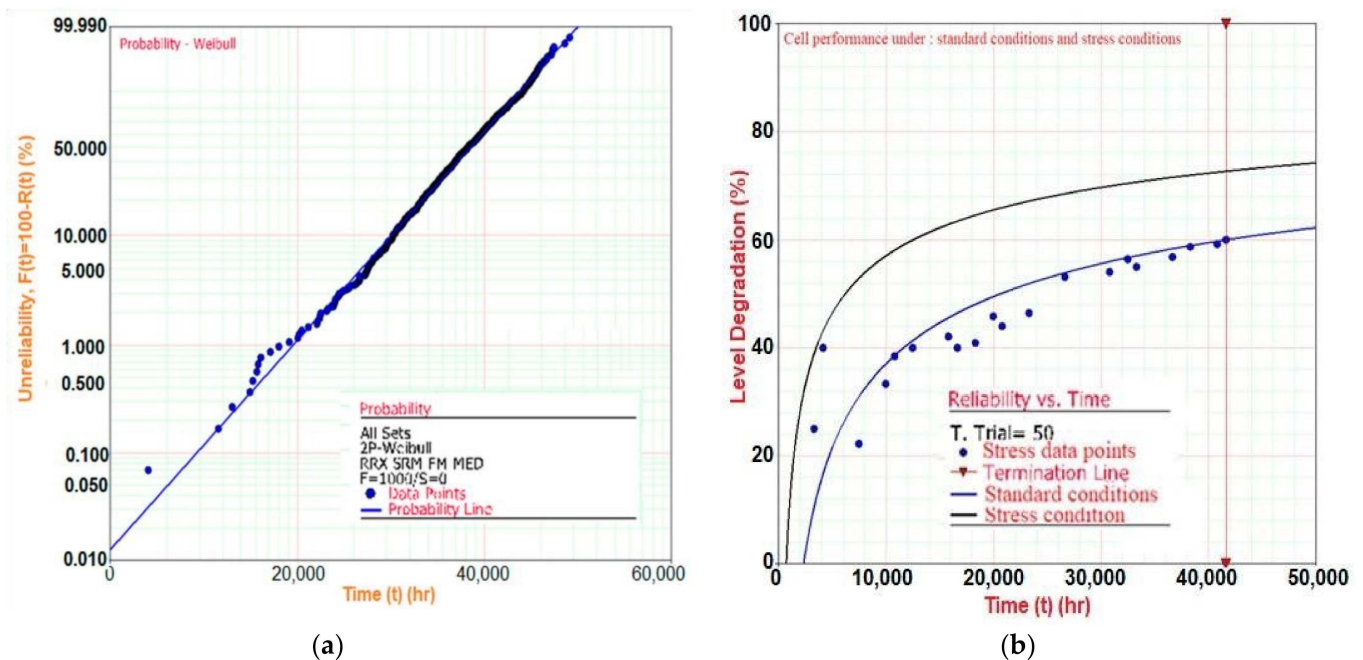


**Figure 21.** (a) Weibull repartition for the studied solar cell lifetime; (b) solar cell degradation degree under standard and stress conditions [105,107].

Using the stress results of the HASS test, it would be possible to determine the following based on ALTA tool numerical simulations: (1) the operating time limiting value in normal conditions (Figure 22a); (2) the probable rate of solar cell failure within the operation temperature range of 50–100 °C (Figure 22b). It is seen that the expected failures' rate dependence increases strongly with temperature.

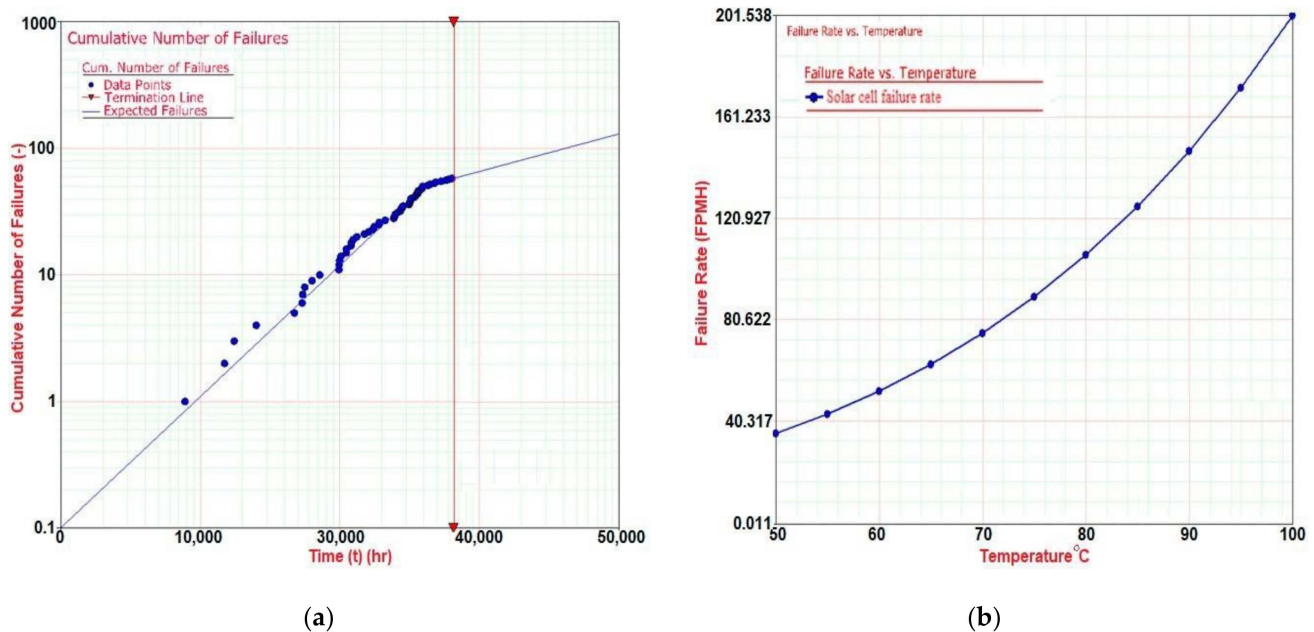


**Figure 22.** (a) Cumulative number of failures as function of time (using ALTA module). (b) Baseline survival of solar cell simulation (using ALTA module) at temperature and stress conditions [105,107].

The simulated results obtained using this reliability analysis consist of (1) identifying the solar cell failure modes; (2) prediction of the solar cell lifetime in normal operation conditions; (3) evaluation of the degradation time and number of defects for the analyzed solar cell.

Based on an experimental approach, it is remarked that the  $\text{Cu}_2\text{O}$ : N layer would be very stable when its annealing for 90 min does not degrade the nitrogen doping [108].

#### 6.4. Reliability of HTSC Based on Si and ZnO

ZnO-based devices improve the reliability of different high performance SCs such as DSSC, Perovskite SC, or OPV SC [109].

The SCs based on ZnO / AZO layers have a good reliability; this feature is very useful for the reliability of HTSC. AZO layers are exposed to specific environmental conditions, namely: (1) high and low levels of temperature such as 100 °C and 20 °C, respectively; (2) high and low levels of humidity, such as 100% and 20%, respectively, or (3) all combinations of temperature and humidity characterized by unchanged microstructure, crystallinity, and optical properties.

## 7. Conclusions and Prospects

### 7.1. Conclusions

Based on the present review article, the following conclusions could be highlighted:

1. Different authors published interesting review articles on HTSC based on Si and metal oxides that presented their own conception [110–113].
2. There were discussed state-of-the-art power conversion efficiencies for HTSC, as well as a comparison analysis with other tandem solar cells such as PSCs.
3. An unified approach of three main essential issues of HTSC was developed, respectively: (a) experimental evaluation based on fabrication and characterization of these solar devices; (b) their modelling and simulation in order to establish optimized solar cells; (c) thermal stability required for industrial applications of HTSC.
4. It was analyzed that the HTSC device architecture stressed on four-terminal tandem configuration combines a conventional crystalline silicon sub-cell with a ZnO/ $\text{Cu}_2\text{O}$  sub-cell in a stack of independently connected cells.

5.  $\text{Cu}_2\text{O}$  and  $\text{ZnO}$  layers could be deposited by different methods, namely: (a) magnetron sputtering; (b) electrodeposition; (c) pulsed laser deposition; (d) plasma deposition; (e) photochemical deposition; (f) atomic layer deposition a.o.
6. Characterization of  $\text{Cu}_2\text{O}$  layer structure was defined by: (a) morphological and structural evaluation (SEM, AFM and XRD); (b) optical evaluation (FTIR Spectroscopy, Spectroscopic Ellipsometry). It was remarked that N-doped cuprous oxide hetero-junction solar cell could be considered as a bright candidate for high-efficiency solar devices.
7. Characterization of  $\text{ZnO}$  layer structure was determined by: (a) structural characterization (SEM, AFM, XRD); (b) optical characterization (UV-VIS Spectroscopy; Photoluminescence Spectroscopy).
8. Numerical modelling of  $\text{Cu}_2\text{O}/\text{ZnO}$  HTSC was studied by: (a) electrical modelling and simulation stressing on J-V characteristics and EQE curve; at the same time, the influence of interface defects on the HTSC efficiency could be put in evidence; (b) optical modelling and simulation would be useful for optical losses' optimization. The performant simulation tools, namely SILVACO and PC1D, could be of great interest for evaluation of optimized parameters.
9. Stability and reliability approach was discussed. The degradation degree of analyzed solar cells, as well as the solar cell lifetime in normal operation conditions, could be established.
10. Tandem Solar Cells like PSCs would be considered to be the most promising candidates for integrating with other systems to realize new innovative technologies. The next-generation applications of perovskite-based solar cells include tandem PV cells, space applications, PV-integrated energy storage systems, PV cell-driven catalysis, and BIPVs. The good stability of these devices would be the main challenge to be considered for future applications.

## 7.2. Prospects

The progress of high-efficiency HTSC with Si-based metal oxides and related perovskite tandem solar cells would contribute to remarkable prospects for these advanced solar devices [114–118]

(a) development of multi-terminal solar cells characterized by a control of interface properties that would allow the reduction of the contribution of defects.

(b) development of high-performance carrier-selective passivating contacts based on tunneling oxide layer combined with conductive organic polymer.

In spite of some drawbacks (these special SCs showed a degradation in performance due to an increased contact resistance at 300–400 °C), they are still maturing and have already shown many successful demonstrations with efficiencies higher than the 20% mark.

(c) development of Si-perovskite tandem solar cells with transition metal oxides as carrier selective contacts.

Using optimized tunnelling and carrier transport layers, efficiency can further be improved for integrated tandem solar cells pointing to practical implications of the proposed structure at an industrial level.

(d) development of reliable and efficient perovskite SCs that require a multilevel approach to optimize the performance of individual layers in each cell separately; the cells are linked together with the substrate.

Researchers at the US National Renewable Energy Laboratory have developed a new concept for manufacturing perovskite solar cells with high efficiency and excellent stability.

**Author Contributions:** Conceptualization, L.F.; methodology, L.F.; formal analysis, L.F.; investigation, L.F. and I.C.; software, A.D., S.F. and D.C.; validation, L.F. and I.C.; resources, L.F. and I.C.; data curation, D.C., A.D. and S.F.; writing—original draft preparation, L.F. and I.C.; writing—review and editing, L.F. and I.C.; visualization, L.F. and I.C.; supervision, L.F.; project administration, L.F. All authors have read and agreed to the published version of the manuscript.

**Funding:** This research received no external funding.

**Institutional Review Board Statement:** Not applicable.

**Informed Consent Statement:** Not applicable.

**Data Availability Statement:** Data supporting reporting results could be found in the following references: 1. Fara, L.; Chilibon, I.; Nordseth, Ø.; Craciunescu, D.; Savastru, D.; Vasiliu, C.; Baschir, L.; Fara, S.; Kumar, R.; Monakhov, E.; Connolly, J.P. Complex Investigation of High Efficiency and Reliable Heterojunction Solar Cell Based on an Improved Cu<sub>2</sub>O Absorber Layer, *Energies* **2020**, *13*, p. 4667; doi:10.3390/en13184667 [37]. 2. Nordseth, O.; Kumar, R.; Bergum, K.; Chilibon, I.; Fara, L.; Foss, S.E.; Monakhov, E. Nitrogen-doped Cu<sub>2</sub>O thin films for photovoltaic applications. *Materials* **2019**, *12*, 3038. [67]. 3. Fara, L.; Craciunescu, D. Reliability analysis of photovoltaic systems for specific applications. In: *Reliability and Ecological Aspects of Photovoltaic Modules*; Gok, A., Ed.; Intech Open: London, UK, 2020; pp. 79–92 [103].

**Acknowledgments:** This review article was determined by: (1) the European Commission COST project “Multiscale in modelling and validation for solar photovoltaics” -Multiscale Solar MP1406, 2015–2019, for PUB and INOE; (2) The European Commission M-ERA.NET project “High-performance tandem heterojunction solar cells for specific applications” -SOLHET, 2016–2019 for IFE, UiO, PUB and INOE. This work was supported by the Romanian Ministry of Research, Innovation and Digitalization (MRID) for: (1) Core Program PN 18N/2019 and PN 23 05 No. 11N /2023 and (2) Program I—Development of the National R & D System, Subprogram 1.2 Institutional Performance-Projects for Excellence Financing in RDI, contr.18PFE/2021.

**Conflicts of Interest:** The authors declare no conflict of interest.

## Abbreviations

ALD	Atomic Layer Deposition
AALD	Atmospheric Atomic Layer Deposition
AFM	Atomic Force Microscopy
AZO	Al-doped ZnO
bcc	body-centered cubic
Cu <sub>2</sub> O	Cuprous oxide
CVD	Chemical Vapor Deposition
d.c. MSP	Direct Current Magnetron Sputtering
EC	European Commission
ECD	Electro-Chemical Deposition
EQE	External quantum efficiency
EVA	Ethylene vinyl acetate
fcc	face-centered cubic
FF	Fill factor
FTIR	Fourier transform infrared spectroscopy
HASS	High accelerated stress screening
HALT	High accelerated life test
HTSC	Tandem heterojunction solar cells
IBS	Ion Beam Sputtering
IDL	Interface defect layer
IEA PVPS	International Energy Agency Photovoltaic Power System Programme
JRC	Joint Research Centre
MSP	Magnetron Sputtering
η	Efficiency
OPV	Organic photovoltaic
PL	Photoluminescence
PLD	Pulsed Laser Deposition
PV	Photovoltaics
r.f. MSP	Radio Frequency Magnetron Sputtering
SC	Solar cell
SE	Spectroscopic Ellipsometry
SEM	Scanning electron microscopy

STHSC	Silicon-based tandem heterojunction solar cell
UV-VIS	Ultraviolet-visible
VAPE	Vacuum Arc Plasma Evaporation
XRD	X-ray diffraction
ZnO	Zinc Oxide

## References

- Available online: <https://ec.europa.eu/energy/en/topics/renewable-energy/renewable-energy-directive> (accessed on 1 June 2021).
- European Commission. The Roadmap for Transforming the EU into a Competitive, Low-Carbon Economy by 2050. Available online: [https://ec.europa.eu/clima/citizens/eu\\_en](https://ec.europa.eu/clima/citizens/eu_en) (accessed on 22 June 2015).
- Proposal for a Directive of the European Parliament and the Council. Directive on the Promotion of the Use of Energy from Renewable Sources (Recast), 2016/0382(COD). Available online: [http://eur-lex.europa.eu/legal-content/EN/TXT/HTML/?uri=CELEX:52016PC0767R\(01\)&from=EN](http://eur-lex.europa.eu/legal-content/EN/TXT/HTML/?uri=CELEX:52016PC0767R(01)&from=EN) (accessed on 30 November 2016).
- Obama, B. The irreversible momentum of clean energy. *Science* **2017**, *355*, 126–129. [[CrossRef](#)] [[PubMed](#)]
- Available online: <http://www.iea-pvps.org> (accessed on 10 April 2018).
- Available online: <http://www.ren21.net> (accessed on 1 March 2022).
- Available online: <https://ec.europa.eu/jrc/en> (accessed on 30 May 2022).
- Gambhir, A.; Sandwel, P.; Nelson, J. The future costs of OPV—A bottom-up model of material and manufacturing costs with uncertainty analysis. *Sol. Energy Mater. Sol. Cells* **2016**, *156*, 49–58. [[CrossRef](#)]
- Petrova-Koch, V.; Hezel, R.; Goetzberger, A. *High Efficient Low-Cost Photovoltaics: Recent Developments*; Springer: Berlin/Heidelberg, Germany, 2008.
- Louwen, A.; van Sark, W.G.J.H.M.; Faaij, A.P.C.; Schropp, R.E.I. Re-assessment of net energy production and greenhouse gas emissions avoidance after 40 years of photovoltaics development. *Nat. Commun.* **2016**, *7*, 13728. [[CrossRef](#)] [[PubMed](#)]
- Yu, X.; Marks, T.J.; Facchetti, A. Metal oxides for optoelectronic applications. *Nat. Mater.* **2016**, *15*, 383–396. [[CrossRef](#)]
- Zielinska-Raczynska, S.; Ziemkiewicz, D.; Czajkowski, G. Electro-optical properties of Cu<sub>2</sub>O for P excitons in the regime of Franz-Keldysh oscillations. *Phys. Rev. B* **2018**, *97*, 165205. [[CrossRef](#)]
- Khattak, Y.H.; Baig, F.; Ullah, S.; Marí, B.; Beg, S.; Khan, K. Effect of Cu<sub>2</sub>O hole transport layer and improved minority carrier life time on the efficiency enhancement of Cu<sub>2</sub>NiSn<sub>4</sub> based experimental solar cell. *J. Renew. Sustain. Energy* **2018**, *10*, 043502. [[CrossRef](#)]
- Tsur, Y.; Riess, I. Self-compensation in semiconductors. *Phys. Rev. B* **1999**, *60*, 8138. [[CrossRef](#)]
- Dong, C.J.; Yu, W.X.; Xu, M.; Cao, J.J.; Chen, C.; Yu, W.W.; Wang, Y.D. Valence band offset of Cu<sub>2</sub>O/In<sub>2</sub>O<sub>3</sub> heterojunction determined by X-ray photoelectron spectroscopy. *J. Appl. Phys.* **2011**, *110*, 073712. [[CrossRef](#)]
- Pavan, M.; Rühle, S.; Ginsburg, A.; Keller, D.A.; Barad, H.-N.; Sberna, P.M.; Nunes, D.; Martins, R.; Anderson, A.Y.; Zaban, A.; et al. TiO<sub>2</sub>/Cu<sub>2</sub>O all-oxide heterojunction solar cells produced by spray pyrolysis. *Sol. Energy Mater. Sol. Cells* **2015**, *132*, 549–556. [[CrossRef](#)]
- Lahmar, H.; Setifi, F.; Azizi, A.; Schmerber, G.; Dinia, A. On the electrochemical synthesis and characterization of p-Cu<sub>2</sub>O/n-ZnO heterojunction. *J. Alloys Compd.* **2017**, *718*, 36–45. [[CrossRef](#)]
- Takiguchi, Y.; Miyajima, S. Device simulation of cuprous oxide heterojunction solar cells. *Jpn. J. Appl. Phys.* **2015**, *54*, 112303. [[CrossRef](#)]
- Nordseth, Ø.; Kumar, R.; Bergum, K.; Fara, L.; Dumitru, C.; Craciunescu, D.; Dragan, F.; Chilibon, I.; Monakhov, E.; Foss, S.E.; et al. Metal Oxide Thin-Film Heterojunctions for Photovoltaic Applications. *Materials* **2018**, *11*, 2593. [[CrossRef](#)]
- Nordseth, Ø.; Kumar, R.; Bergum, K.; Fara, L.; Foss, S.E.; Haug, H.; Dragan, F.; Craciunescu, D.; Sterian, P.; Chilibon, I.; et al. Optical analysis of a ZnO/Cu<sub>2</sub>O subcell in a silicon-based tandem heterojunction solar cell. *Green Sustain. Chem.* **2017**, *7*, 57–69. [[CrossRef](#)]
- Minami, T.; Nishi, Y.; Miyata, T. Efficiency enhancement using a Zn<sub>1-x</sub>Ge<sub>x</sub>O thin film as an n-type window layer in Cu<sub>2</sub>O based heterojunction solar cells. *Appl. Phys. Express* **2016**, *9*, 052301. [[CrossRef](#)]
- Gunnæs, A.E.; Gorantla, S.; Løvvik, O.M.; Gan, J.; Carvalho, P.A.; Svensson, B.G.; Monakhov, E.V.; Bergum, K.; Jensen, I.T.; Diplas, S. Epitaxial Strain-Induced Growth of CuO at Cu<sub>2</sub>O/ZnO Interfaces. *J. Phys. Chem. C* **2016**, *120*, 23552–23558. [[CrossRef](#)]
- White, P.T.; Niraj, L.N.; Kylie, C.R. Tandem Solar Cells Based on High-Efficiency c-Si Bottom Cells: Top Cell Requirements for >30% Efficiency. *IEEE J. Photovolt.* **2014**, *4*, 208–214. Available online: <https://ieeexplore.ieee.org/document/6626569> (accessed on 9 October 2013). [[CrossRef](#)]
- Jacobsen, E.C. Analysis of the ZnO/Cu<sub>2</sub>O Thin Film Heterojunction for Intermediate Band Solar Cell Applications, see the Chapters 3–6, Respectively: Literature Review, Proposed Design, Methodology and Experimental Setups, Experimental Results and Discussion. Master's Thesis, NTNU-Norwegian University of Science and Technology, Trondheim, Norway, June 2015; 113p. Available online: <https://core.ac.uk/download/pdf/154672771.pdf> (accessed on 1 June 2015).
- Tsakalagos, L. (Ed.) *Nanotechnology for Photovoltaics*; CRC Press: Boca Raton, FL, USA, 2010; Taylor and Francis Group: Abingdon, UK, 2010; 458p. [[CrossRef](#)]
- De Vos, A. Detailed balance limit of the efficiency of tandem solar cells. *J. Phys. D Appl. Phys.* **1980**, *13*, 839. [[CrossRef](#)]

27. National Renewable Energy Laboratory. *Research Cell Efficiency Records*; National Renewable Energy Laboratory: Washington, DC, USA, 2015.
28. Nordseth, Ø.; Fara, L.; Kumar, R.; Foss, S.E.; Dumitru, C.; Muscuirel, V.-F.; Drăgan, F.; Crăciunescu, D.; Bergum, K.; Haug, H.; et al. Electro-optical modeling of a ZnO/Cu<sub>2</sub>O subcell in a silicon-based tandem heterojunction solar cell. In Proceedings of the 33rd European Photovoltaic Solar Energy Conference and Exhibition, Amsterdam, The Netherlands, 25–29 September 2017; pp. 172–177.
29. Bergum, K.; Riise, H.N.; Gorantla, S.; Lindberg, P.F.; Jensen, I.J.T.; Gunnæs, A.E.; Galeckas, A.; Diplas, S.; Svensson, B.G.; Monakhov, E. Improving carrier transport in Cu<sub>2</sub>O thin films by rapid thermal annealing. *J. Phys. Condens. Matter* **2018**, *30*, 075702. [CrossRef]
30. Gan, J.; Venkatachalapathy, V.; Svensson, B.G.; Monakhov, E. Influence of target power on properties of Cu<sub>x</sub>O thin films prepared by reactive radio frequency magnetron sputtering. *Thin Solid Films* **2015**, *594*, 250–255. [CrossRef]
31. Ashida, A.; Sato, S.; Yoshimura, T.; Fujimura, N. Control of native acceptor density in epitaxial Cu<sub>2</sub>O thin films grown by electrochemical deposition. *J. Cryst. Growth* **2017**, *468*, 245–248. [CrossRef]
32. Kwon, J.-D.; Kwon, S.-H.; Jung, T.-H.; Nam, K.-S.; Chung, K.-B.; Kim, D.-H.; Park, J.-S. Controlled growth and properties of p-type cuprous oxide films by plasma enhanced atomic layer deposition at low temperature. *Appl. Surf. Sci.* **2013**, *285*, 373–379. [CrossRef]
33. Avila, J.R.; Peters, A.W.; Li, Z.Y.; Ortuno, M.A.; Martinson, A.B.F.; Cramer, C.J.; Hupp, J.T.; Farha, O.K. Atomic layer deposition of Cu(I) oxide films using Cu(II) bis(dimethylamino-2-propoxide) and water. *Dalton Trans.* **2017**, *46*, 5790–5795. [CrossRef] [PubMed]
34. Izaki, M.; Mizuno, K.-T.; Shinagawa, T.; Inaba, M.; Tasaka, A. Photochemical construction of photovoltaic device composed of p-copper(I) oxide and n-zinc oxide. *J. Electrochem. Soc.* **2006**, *153*, C668–C672. [CrossRef]
35. Jeong, S.; Aydil, E.S. 2010 Structural and electrical properties of Cu<sub>2</sub>O thin films deposited on ZnO by metal organic chemical vapor deposition. *J. Vac. Sci. Technol. A* **2010**, *28*, 1338–1343. [CrossRef]
36. Siddiqui, H.; Parra, M.R.; Pandey, P.; Singh, N.; Qureshi, M.S.; Haque, Z. A review: Synthesis, characterization and cell performance of Cu<sub>2</sub>O based material for solar cells. *Orient. J. Chem.* **2012**, *28*, 1533–1545. [CrossRef]
37. Available online: <http://www.sputtering-targets.net/blog/advantages-and-disadvantages-of-pulsed-laser-deposition-pld/> (accessed on 8 August 2018).
38. Available online: <https://julissazhang.wixsite.com/sputtertargets/single-post/2019/12/10/advantages-and-disadvantages-of-magnetron-sputtering> (accessed on 1 August 2018).
39. Available online: <https://www.universitywafer.com/advantages-disadvantages-mocvd.html#:~:text=Metal%20Organic%20Chemical%20Vapor%20Deposition%20Advantages%20and%20Disadvantages,process%20include%20achieving%20a%20uniform%2C%20high-conductivity%20thin%20film> (accessed on 1 March 2022).
40. Available online: [https://www.researchgate.net/publication/332277595\\_New\\_Development\\_of\\_Atomic\\_Layer\\_Deposition\\_Processes\\_Methods\\_and\\_Applications](https://www.researchgate.net/publication/332277595_New_Development_of_Atomic_Layer_Deposition_Processes_Methods_and_Applications) (accessed on 1 April 2019).
41. Ozaveshe Oviroh, P.; Rokhsareh, A.; Pan, D.; Coetzee, R.A.; Jen, T.C. New development of atomic layer deposition: Processes, methods and applications. *Sci. Technol. Adv. Mater.* **2019**, *20*, 465–496. [CrossRef]
42. Fara, L.; Chilibon, I.; Nordseth, Ø.; Craciunescu, D.; Savastru, D.; Vasiliu, C.; Baschir, L.; Fara, S.; Kumar, R.; Monakhov, E.; et al. Complex Investigation of High Efficiency and Reliable Heterojunction Solar Cell Based on an Improved Cu<sub>2</sub>O Absorber Layer. *Energies* **2020**, *13*, 4667. [CrossRef]
43. Minami, T.; Miyata, T.; Ihara, K.; Minamino, Y.; Tsukada, S. Effect of ZnO film deposition methods on the photovoltaic properties of ZnO–Cu<sub>2</sub>O heterojunction devices. *Thin Solid Films* **2006**, *494*, 47–52. [CrossRef]
44. Al-Ghamdi, A.A.; Al-Hartomy, O.A.; El Okr, M.; Nawar, A.M.; El-Gazzar, S.; El-Tantawy, F.; Yakuphanoglu, F. Semiconducting properties of Al doped ZnO thin films. *Spectrochim. Acta Part A Mol. Biomol. Spectrosc.* **2014**, *131*, 512–517. [CrossRef]
45. Pal, D.; Singhal, J.; Mathur, A.; Singh, A.; Dutta, S.; Zollner, S.; Chattopadhyay, S. Effect of substrates and thickness on optical properties in atomic layer deposition grown ZnO thin films. *Appl. Surf. Sci.* **2017**, *421*, 341–348. [CrossRef]
46. Habibi, A.; Vatandoust, L.; Aref, S.M.; Naghshara, H. Formation of high performance nanostructured ZnO thin films as a function of annealing temperature: Structural and optical properties. *Surf. Interfaces* **2020**, *21*, 100723. [CrossRef]
47. Ievskaya, Y.; Hoye, R.L.Z.; Sadhanala, A.; Musselman, K.P.; MacManus-Driscoll, J.L. Fabrication of ZnO/Cu<sub>2</sub>O heterojunctions in atmospheric conditions: Improved interface quality and solar cell performance. *Sol. Energy Mater. Sol. Cells* **2015**, *135*, 43–48. [CrossRef]
48. Minami, T.; Nishi, Y.; Miyata, T. High-efficiency Cu<sub>2</sub>O-based heterojunction solar cells fabricated using a Ga<sub>2</sub>O<sub>3</sub> thin film as ntype layer. *Appl. Phys. Express* **2013**, *6*, 044101. [CrossRef]
49. Minami, T.; Nishi, Y.; Miyata, T.; Abe, S. Photovoltaic properties in Al doped ZnO/non-doped Zn<sub>1-x</sub>Mg<sub>x</sub>O/Cu<sub>2</sub>O heterojunction solar cells. *ECS Trans.* **2012**, *50*, 59–68. [CrossRef]
50. Nishi, Y.; Miyata, T.; Minami, T. The impact of heterojunction formation temperature on obtainable conversion efficiency in n-ZnO/p-Cu<sub>2</sub>O solar cells. *Thin Solid Films* **2013**, *528*, 72–76. [CrossRef]
51. Lee, Y.S.; Chua, D.; Brandt, R.E.; Siah, S.C.; Li, J.V.; Mailoa, J.P.; Lee, S.W.; Gordon, R.G.; Buonassisi, T. Atomic layer deposited gallium oxide buffer layer enables 1.2 V open-circuit voltage in cuprous oxide solar cells. *Adv. Mater.* **2014**, *26*, 4704–4710. [CrossRef]

52. Minami, T.; Nishi, Y.; Miyata, T.; Nomoto, J. High-Efficiency Oxide Solar Cells with ZnO/Cu<sub>2</sub>O Heterojunction Fabricated on Thermally Oxidized Cu<sub>2</sub>O Sheets. *Appl. Phys. Express* **2011**, *4*, 062301. [CrossRef]
53. Lee, S.W.; Lee, Y.S.; Heo, J.; Siah, S.C.; Chua, D.; Brandt, R.E.; Kim, S.B.; Mailoa, J.P.; Buonassisi, T.; Gordon, R.G. Improved Cu<sub>2</sub>O-based solar cells using atomic layer deposition to control the Cu oxidation state at the p–n junction. *Adv. Energy Mater.* **2014**, *4*, 1301916. [CrossRef]
54. Lee, Y.S.; Heo, J.; Siah, S.C.; Mailoa, J.P.; Brandt, R.E.; Kim, S.B.; Gordon, R.G.; Buonassisi, T. Ultrathin amorphous zinc-tin oxide buffer layer for enhancing heterojunction interface. *Energy Environ. Sci.* **2013**, *6*, 2112–2118. [CrossRef]
55. Boughelout, A.; Makaluso, R.; Crupi, I.; Megna, B.; Aida, M.S.; Kecchouane, M. Improved Cu<sub>2</sub>O/AZO Heterojunction by Inserting a Thin ZnO Interlayer Grown by Pulsed Laser Deposition. *J. Electron. Mater.* **2019**, *48*, 4381–4388. [CrossRef]
56. Mittiga, A.; Salza, E.; Sarto, F.; Tucci, M.; Vasanthi, R. Heterojunction solar cell with 2% efficiency based on a Cu<sub>2</sub>O substrate. *Appl. Phys. Lett.* **2006**, *88*, 163502. [CrossRef]
57. Salisu, I.K.; Yunusa, A.; Mustafa, M.K.; Ahmad, M.K. and Mohd Khairul, A. Cuprous Oxide (Cu<sub>2</sub>O) Based Solar Cell Thickness Dependence. *Br. J. Phys. Stud.* **2022**, *1*, 1–7. [CrossRef]
58. Minami, T.; Tanaka, H.; Shimakawa, T.; Sato, H.; Miyata, T. High-efficiency oxide heterojunction solar cells using Cu<sub>2</sub>O sheets. *Jpn. J. Appl. Phys.* **2004**, *43*, L917–L919. [CrossRef]
59. Hussain, S.; Cao, C.; Nabi, G.; Khan, W.S.; Usman, Z.; Mahmood, T. Effect of electrodeposition and annealing of ZnO on optical and photovoltaic properties of the p-Cu<sub>2</sub>O/n-ZnO solar cells. *Electrochim. Acta* **2011**, *56*, 8342–8346. [CrossRef]
60. Katayama, J.; Ito, K.; Matsuoka, M.; Tamaki, J. Performance of Cu<sub>2</sub>O/ZnO solar cell prepared by two-step electrodeposition. *J. Appl. Electrochem.* **2004**, *34*, 687–692. [CrossRef]
61. Fujimoto, K.; Oku, T.; Akiyama, T. Fabrication and characterization of ZnO/Cu<sub>2</sub>O solar cells prepared by electrodeposition. *Appl. Phys. Express* **2013**, *6*, 086503. [CrossRef]
62. Izaki, M.; Shinagawa, T.; Mizuno, K.-T.; Ida, Y.; Inaba, M.; Tasaka, A. Electrochemically constructed p-Cu<sub>2</sub>O/n-ZnO heterojunction diode for photovoltaic device. *J. Phys. D Appl. Phys.* **2007**, *40*, 3326–3329. [CrossRef]
63. Marin, A.T.; Muñoz-Rojas, D.; Iza, D.C.; Gershon, T.; Musselman, K.P.; MacManus-Driscoll, J.L. Novel atmospheric growth technique to improve both light absorption and charge collection in ZnO/Cu<sub>2</sub>O thin film solar cells. *Adv. Funct. Matter* **2013**, *23*, 3413–3419. [CrossRef]
64. Musselman, K.P.; Wisnet, A.; Iza, D.C.; Hesse, H.C.; Scheu, C.; MacManus-Driscoll, J.L.; Schmidt-Mende, L. Strong efficiency improvements in ultra-low-cost inorganic nanowire solar cells. *Adv. Mater.* **2010**, *22*, E256–E258. [CrossRef]
65. Jeong, S.S.; Mittiga, A.; Salza, A.; Masci, A.; Passerini, A. Electrodeposited ZnO/Cu<sub>2</sub>O heterojunction solar cells. *Electrochim. Acta* **2008**, *53*, 2226–2231. [CrossRef]
66. World Intellectual Property Organization. Solar Cell, Multijunction Solar Cell, Solar Cell Module and Solar Power Generation System, WIPO/PCT, Japan. Patent. WO2019058605A1, 28 March 2019. Available online: <https://patentimages.storage.googleapis.com/2e/f5/dc/eb1e0778922963/WO2019058605A1.pdf> (accessed on 28 March 2019).
67. Wang, Y.; Ghanbaja, J.; Horwat, D.; Yu, L.; Pierson, J.F. Nitrogen chemical state in N-doped Cu<sub>2</sub>O thin films. *Appl. Phys. Lett.* **2017**, *110*, 131902. [CrossRef]
68. Nordseth, Ø.; Chilibon, I.; Kumar, R.; Bergum, K.; Vasiliu, C.; Iordanescu, R.; Baschir, L.; Savastru, D.; Kiss, A.; Parau, A.; et al. Characterization of Cuprous Oxide Thin Films Prepared by Reactive Direct Current Magnetron Sputtering. *Sens. Transducers* **2018**, *220*, 37–44.
69. Bennett, J.M.; Mattson, L. *Introduction to Surface Roughness and Scattering*; Optical Society of America: Washington, DC, USA, 1989.
70. Nordseth, O.; Kumar, R.; Bergum, K.; Chilibon, I.; Fara, L.; Foss, S.E.; Monakhov, E. Nitrogen-doped Cu<sub>2</sub>O thin films for photovoltaic applications. *Materials* **2019**, *12*, 3038. [CrossRef]
71. *JCPDS 78-2076 for Cu<sub>2</sub>O*; International Centre for Diffraction Data-JCPDS: Newtown Square, PA, USA, 1996.
72. Nakano, Y.; Saeki, S.; Morikawa, T. Optical bandgap widening of p-type Cu<sub>2</sub>O films by nitrogen doping. *Appl. Phys. Lett.* **2009**, *94*, 022111. [CrossRef]
73. Reddy, M.H.P.; Pierson, J.F.; Uthanna, S. Structural, surface morphological, and optical properties of nanocrystal line Cu<sub>2</sub>O and CuO films formed by RF magnetron sputtering: Oxygen partial pressure effect. *Phys. Status Solidi A* **2012**, *209*, 1279–1286. [CrossRef]
74. Sberna, P.M.; Crupi, I.; Moscatelli, F.; Privitera, V.; Simone, F.; Miritello, M. Sputtered cuprous oxide thin films and nitrogen doping by ion implantation. *Thin Solid Films* **2016**, *600*, 71–75. [CrossRef]
75. Ogwu, A.A.; Darma, T.H. A reactive magnetron sputtering route for attaining a controlled core-rim phase partitioning in Cu<sub>2</sub>O/CuO thin films with resistive switching potential. *J. Appl. Phys.* **2013**, *113*, 183522. [CrossRef]
76. Su, J.; Niu, Q.; Sun, R.; An, X.; Zhang, Y. Investigation of Cu<sub>2</sub>O films sputtered with ceramic target: Effect of RF power. *J. Optoelectron. Adv. Mater.* **2018**, *20*, 441–444.
77. Gong, J.B.; Dong, W.L.; Dai, R.C.; Wang, Z.P.; Zhang, Z.M.; Ding, Z.J. Thickness dependence of the optical constants of oxidized copper thin films based on ellipsometry and transmittance. *Chin. Phys. B* **2014**, *23*, 087802. [CrossRef]
78. Liao, L.C.-K.; Tang, C.-H. Effect of a Cu<sub>2</sub>O buffer layer on the efficiency in p-Cu<sub>2</sub>O/ZnO hetero-junction photovoltaics using electrochemical deposition processing. *J. Appl. Electrochem.* **2022**, *52*, 1459–1467. [CrossRef]
79. Li, J.; Mei, Z.; Liu, L.; Liang, H.; Azarov, A.; Kuznetsov, A.; Liu, Y.; Ji, A.; Meng, Q.; Du, X. Probing defects in nitrogen-doped Cu<sub>2</sub>O. *Sci. Rep.* **2014**, *4*, 7240. [CrossRef] [PubMed]

80. Hashim, M.S.; Khaleel, R.S. The bioactivities of prepared Ti, Zn, TiO<sub>2</sub>, ZnO and Al<sub>2</sub>O<sub>3</sub> nanoparticles by rapid breakdown anodization technique. *Surf. Interfaces* **2020**, *20*, 100640. [CrossRef]
81. Powder Diffraction Journal-Volume 1-ICDD. Available online: <https://www.icdd.com/powder-diffraction-journal-volume-1/> (accessed on 25 April 2020).
82. Full text of "Standard X-ray Diffraction Powder Patterns:-13-Data for 58 Substances". Available online: [https://archive.org/stream/standardxraydiff2513morr/standardxraydiff2513morr\\_djvu.txt](https://archive.org/stream/standardxraydiff2513morr/standardxraydiff2513morr_djvu.txt) (accessed on 25 April 2020).
83. Özdoğan, M.; Yiğen, S.; Çelebi, C.; Utlu, G. The comparison of transient photocurrent spectroscopy measurements of Pulsed Electron Deposited ZnO thin film for air and vacuum ambient conditions. *Thin Solid Films* **2019**, *680*, 48–54. [CrossRef]
84. Zou, T.; Huang, J.; Hu, Y.; Tang, K.; Zhang, Z.; Zhou, X.; Shen, Y.; Zhang, J.; Wang, L.; Lu, Y. CdZnTe thick film radiation detectors with B and Ga co-doped ZnO contacts. *Surf. Coat. Technol.* **2019**, *360*, 64–67. [CrossRef]
85. Singh, G.; Pandey, P.M. Uniform and graded copper open cell ordered foams fabricated by rapid manufacturing: Surface morphology, mechanical properties and energy absorption capacity. *Mater. Sci. Eng. A* **2019**, *761*, 138035. [CrossRef]
86. Urper, O.; Baydogan, N. Effect of Al concentration on optical parameters of ZnO thin film derived by Sol-Gel dip coating technique. *Mater. Lett.* **2020**, *274*, 128000. [CrossRef]
87. Chou, H.S.; Di Yang, K.; Xiao, S.H.; Patil, R.A.; Lai, C.C.; Vincent Yeh, W.C.; Ho, C.H.; Liou, Y.; Ma, Y.R. Temperature dependent ultraviolet photoluminescence in hierarchical Zn, ZnO and ZnO/Zn nanostructures. *Nanoscale* **2019**, *11*, 13385–13396. [CrossRef]
88. Munawar, T.; Iqbal, F.; Yasmeen, S.; Mahmood, K.; Hussain, A. Multi metal oxide NiOCdO-ZnO nanocomposite—synthesis, structural, optical, electrical properties and enhanced sunlight driven photocatalytic activity. *Ceram. Int.* **2020**, *46*, 2421–2437. [CrossRef]
89. Giannouli, M. Current Status of Emerging PV Technologies: A Comparative Study of Dye-Sensitized, Organic, and Perovskite Solar Cells. *Int. J. Photoenergy* **2021**, *2021*, 6692858. [CrossRef]
90. Auf der Maur, M. Multiscale Approaches for the Simulation of Optoelectronics Devices. *J. Green Eng.* **2016**, *5*, 133–156. [CrossRef]
91. Aeberhard, U.; Czaja, P.; Ermes, M.; Pieters, B.E.; Chistiakova, G.; Bittkau, K.; Richter, A.; Ding, K.; Giusepponi, S.; Celino, M. Towards a Multiscale Approach to the Simulation of Silicon Hetero-junction Solar Cells. *J. Green Eng.* **2016**, *5*, 11–32. [CrossRef]
92. Connolly, J.P.; Koduvelikulathu, L.J.; Mencaraglia, D.; Rimada, J.C.; Nejim, A.; Sanchez, G. Multiscale approaches to high efficiency photovoltaics. *Renew. Energy Environ. Sustain.* **2016**, *1*, 6. [CrossRef]
93. Lloyd, M.A.; Siah, S.C.; Brandt, R.E.; Serdy, J.; Johnson, S.W.; Lee, Y.S.; Buinassisi, T. Intrinsic defect engineering of cuprous oxide to enhance electrical transport properties for photovoltaic applications. In Proceedings of the IEEE 40th Photovoltaic Specialists Conference (PVSC), Denver, CO, USA, 8–13 June 2014; pp. 3443–3445.
94. Tolstova, Y.; Omelchenko, S.T.; Blackwell, R.E.; Shing, A.M. Polycrystalline Cu<sub>2</sub>O photovoltaic devices incorporating Zn (O, S) window layers. *Sol. Energy Mat. Sol. Cells* **2017**, *160*, 340–345. [CrossRef]
95. Robertson, J.; Falabretti, B. Band o sets of high K gate oxides on III-V semiconductors. *J. Appl. Phys.* **2006**, *100*, 014111. [CrossRef]
96. Brandt, R.E.; Young, M.; Hejin, H.P.; Dameron, A.; Chua, D.; Lee, S.Y.; Teeter, G.; Gordon, R.; Buonassisi, T. Band o\_sets of ntype electron-selective contacts on cuprous oxide (Cu<sub>2</sub>O) for photovoltaics. *Appl. Phys. Lett.* **2014**, *105*, 263901. [CrossRef]
97. PV Lighthouse. Available online: <https://www.pvlighthouse.com.au/> (accessed on 20 January 2020).
98. Baker-Finch, S.C.; McIntosh, K.R. OPAL 2: Rapid optical simulation of silicon solar cells. In Proceedings of the 38th IEEE Photovoltaic Specialists Conference, Austin, TX, USA, 3–8 June 2012; pp. 265–271.
99. Dumitru, C.; Muscurel, V.; Nordseth, O.; Fara, L.; Sterian, P. Optimization of electro-optical performance and material parameters for a tandem metal oxide solar cell. In Proceedings of the International Conference on Computational Science and Its Applications—ICCSA, Melbourne, Australia, 2–5 July 2018; pp. 573–582.
100. Murali, D.S.; Kumar, S.; Choudhary, R.J.; Wadikar, A.D.; Jain, M.K.; Subrahmanyam, A. Synthesis of Cu<sub>2</sub>O from CuO thin films: Optical and electrical properties. *AIP Adv.* **2015**, *5*, 047143. [CrossRef]
101. Todorov, T.K.; Reuter, K.B.; Mitzi, D.B. High-efficiency solar cell with earth-abundant liquid-processed absorber. *Adv. Mater.* **2010**, *22*, E156–E159. [CrossRef]
102. Hodes, G.; Cahen, D. Photovoltaics: Perovskite cells roll forward. *Nat. Photonics* **2014**, *8*, 87–88. [CrossRef]
103. Hailegnaw, B.; Kirmayer, S.; Edri, E.; Hodes, G.; Cahen, D. Rain on methylammonium lead iodide based perovskites: Possible environmental effects of perovskite solar cells. *J. Phys. Chem. Lett.* **2015**, *6*, 153–157. [CrossRef]
104. Reliability Engineering Software Products—ReliaSoft. Available online: <https://www.reliasoft.com.reliasoft.com> (accessed on 20 January 2019).
105. Sharma, V.; Chandel, S.S. Performance and degradation analysis for long term reliability of solar photovoltaic systems: A review. *Renew. Sustain. Energy Rev.* **2013**, *27*, 753–767. [CrossRef]
106. Guo, D.; Brinkman, D.; Shaik, A.R.; Ringhofer, C.; Vasileska, D. Metastability and reliability of CdTe solar cells. *J. Phys. D Appl. Phys.* **2018**, *51*, 153002. [CrossRef]
107. Fara, L.; Craciunescu, D. Reliability analysis of photovoltaic systems for specific applications. In *Reliability and Ecological Aspects of Photovoltaic Modules*; Gok, A., Ed.; Intech Open: London, UK, 2020; pp. 79–92.
108. Ye, F.; Zeng, J.J.; Qiu, Y.B.; Cai, X.M.; Wang, B.; Wang, H.; Zhang, D.P.; Fan, P.; Roy, V.A.L. Deposition-rate controlled nitrogen-doping into cuprous oxide and its thermal stability. *Thin Solid Films* **2019**, *674*, 44–51. [CrossRef]
109. Wibowo, A.; Marsudi, M.A.; Amal, M.I.; Ananda, M.B.; Stephanie, R.; Ardy, H.; Diguna, L.J. ZnO nanostructured materials for emerging solar cell applications. *RSC Adv.* **2020**, *10*, 42838–42859. [CrossRef]

110. Abdu, Y.; Musa, A.O. Copper (I) oxide (Cu<sub>2</sub>O) based solar cells-A review. *Bayero J. Pure Appl. Sci.* **2009**, *2*, 8–12.
111. Chevallier, C.; Bose, S.; Hamady, S.O.S.; Fressengeas, N. Numerical investigations of the impact of buffer germanium composition and low cost fabrication of Cu<sub>2</sub>O on AZO/ZnGeO/Cu<sub>2</sub>O solar cell performances. *EPJ Photovolt.* **2021**, *12*, 3. [[CrossRef](#)]
112. Soonmin, H. A Review of Metal Oxide Thin Films in Solar Cell Applications. *Int. J. Thin Film Sci. Technol.* **2022**, *11*, 37–45. [[CrossRef](#)]
113. Liu, Y.; Li, Y.; Wu, Y.; Yang, G.; Mazzarella, L.; Procel-Moya, P.; Tamboli, A.C.; Weber, K.; Boccard, M.; Isabella, O.; et al. High-Efficiency Silicon Heterojunction Solar Cells: Materials, Devices and Applications. *Mater. Sci. Eng. R* **2020**, *142*, 100579. [[CrossRef](#)]
114. Ehsan, R.; Zubair, A. Review on two-terminal and four-terminal crystalline-silicon/perovskite tandem solar cells; progress, challenges, and future perspectives. *Energy Rep.* **2022**, *8*, 5820–5851. [[CrossRef](#)]
115. Park, J.H.; Ji, S.G.; Park, I.J.; Hwang, S.K.; Lim, H.W.; Kim, J.Y. Sub-cell characterization of two-terminal perovskite/silicon tandem solar cells. *Cell Rep. Phys. Sci.* **2022**, *3*, 101076. [[CrossRef](#)]
116. Chander, S.; Kant Tripathi, S. Recent advancement in efficient metal oxide-based flexible perovskite solar cells: A short review. *Mater. Adv.* **2022**, *3*, 7198–7211. [[CrossRef](#)]
117. McMahon, W.E.; Geisz, J.F.; Buencuerpo, J.; Warren, E.L. A framework for comparing the energy production of photo voltaic modules using 2-, 3-, and 4-terminal tandem cells. *Sustain. Energy Fuels* **2023**, *7*, 461–470. [[CrossRef](#)]
118. Available online: [https://www.researchgate.net/publication/359389404\\_Analysis\\_of\\_Silicon-perovskite\\_Tandem\\_Solar\\_Cells\\_with\\_Transition\\_Metal\\_Oxides\\_as\\_Carrier\\_Selective\\_Contact\\_Layers](https://www.researchgate.net/publication/359389404_Analysis_of_Silicon-perovskite_Tandem_Solar_Cells_with_Transition_Metal_Oxides_as_Carrier_Selective_Contact_Layers) (accessed on 1 March 2022).

**Disclaimer/Publisher’s Note:** The statements, opinions and data contained in all publications are solely those of the individual author(s) and contributor(s) and not of MDPI and/or the editor(s). MDPI and/or the editor(s) disclaim responsibility for any injury to people or property resulting from any ideas, methods, instructions or products referred to in the content.